Mon. Not. R. Astron. Soc. **000**, 1–23 (2004) Printed 30 September 2018 (MN LATEX style file v1.4)

Group, field and isolated early-type galaxies II. Global trends from nuclear data

G. Denicoló,[1⋆] Roberto Terlevich,[2†] Elena Terlevich,[2†] Duncan A. Forbes,[3] Alejandro Terlevich[4]

[1] *Institute of Astronomy, Madingley Road, Cambridge, CB3 0HA, United Kingdom*
[2] *Instituto Nacional de Astrofísica, Óptica y Electrónica, Tonantzintla, Puebla, Mexico*
[3] *Centre for Astrophysics & Supercomputing, Swinburne University, Hawthorn, VIC 3122, Australia*
[4] *School of Physics and Astronomy, University of Birmingham, Edgbaston, Birmingham, B15 2TT, United Kingdom*

Accepted. Received; in original form 2004 July

ABSTRACT

We have derived ages, metallicities and enhanced-element ratios [α/Fe] for a sample of 83 early-type galaxies essentially in groups, the field or isolated objects. The stellar population properties derived for each galaxy corresponds to the nuclear $r_e/8$ aperture extraction. The median age found for Es is 5.8 ± 0.6 Gyr and the average metallicity is +0.37 ± 0.03 dex. For S0s, the median age is 3.0 ± 0.6 Gyr and [Z/H] = 0.53 ± 0.04 dex. We compare the distribution of our galaxies in the Hβ-[MgFe] diagram with Fornax galaxies. Our elliptical galaxies are 3-4 Gyr younger than Es in the Fornax cluster. We find that the galaxies lie in a plane defined by [Z/H] = 0.99 log σ_0 - 0.46 log *Age* - 1.60, or in linear terms $Z \propto \sigma_0 \cdot \mathrm{Age}^{-0.5}$. More massive (larger σ_0) and older galaxies present, on average, large [α/Fe] values, and therefore, must have undergone shorter star-formation timescales. Comparing group against field/isolated galaxies, it is not clear that environment plays an important role in determining their stellar population history. In particular, our isolated galaxies show ages differing in more than 8 Gyr. Finally we explore our large spectral coverage to derive log(O/H) metallicity from the Hα and [N II] λ6584 Å and compare it with model-dependent [Z/H]. We find that the O/H abundances are similar for all galaxies, and we can interpret it as if most chemical evolution has already finished in these galaxies.

Key words: galaxies: stellar content – galaxies: abundances – galaxies: elliptical and lenticular – galaxies: nuclei – galaxies: evolution

1 INTRODUCTION

A decision over the most appropriate scenario of formation and evolution of early-type galaxies is still an open question despite the enormous amount of work already put forward to model primary observational constraints and scaling relations. Most recent flavours of models ranging from monolithic collapse scenarios to hierarchical clustering predictions include Arimoto & Yoshii (1987, 1989); Kauffmann, White & Guiderdoni 1993; Bruzual & Charlot (1993); Bressan, Chiosi & Fagotto (1994); Worthey (1994); Einsel *et al.* (1995); Navarro *et al.* (1996); Steinmetz (1996); Tantalo *et al.* (1996); Bressan, Chiosi & Tantalo (1996); Gibson (1996a,b, 1998); Gibson & Matteucci (1997); Tantalo, Chiosi & Bressan (1998); Chiosi & Carraro (2002); Terlevich & Forbes (2002); and references therein.

Briefly, in the conventional monolithic collapse scenario elliptical galaxies formed as a result of a single violent burst of star formation at high redshift (possibly $z > 3$) and evolved quiescently ever since. By contrast, in the Hierarchical model, there is no intrinsic difference between star formation occurring at different epochs. All galaxies are viewed as similar star-forming systems in which there is an equilibrium between the inflow of gas and the rate at which it is either consumed or driven out of the galaxies by a supernova wind. Elliptical galaxies are formed by merger and/or accretion of smaller units over a time scale comparable to the Hubble time.

As pointed out by Trager *et al.* (2000b, hereafter T00b), the evidence for intermediate-age stellar population (between 1 and 10 Gyr) would favour hierarchical models, which more naturally have extended star formation over time. On

⋆ Visitor at INAOE, Mexico.
† Visiting Fellow, IoA, Cambridge. E-mail for contact: *rjt@inaoep.mx* and *eterlevi@inaoep.mx*

the other hand, Willis et al. (2002) have presented an analysis of the mean star formation history and space density of a sample of luminous field (in their definition, field is equivalent to non-cluster) early-type galaxies selected over the redshift interval $0.3 \lesssim z \lesssim 0.6$. In all, the mean star formation history of the sample is characterised by an apparently old ($z_f > 1$), solar to slightly above-solar metallicity luminosity-weighted stellar population that has evolved passively since the formation epoch. The mean properties of Willis et al. sample are markedly similar to the properties of morphologically-selected luminous elliptical galaxies in rich cluster environments at redshifts $z < 1$ (Ferreras *et al.* 1999). Though neither result in isolation constrains the extent to which early-type galaxies in field or cluster environments represent a co-eval or co-metal population, the broad similarity between the star formation history of the dominant stellar mass component in such galaxies is consistent with similar formation conditions for each population.

Furthermore, the recent results from the K20 survey (Cimatti *et al.* 2002) have identified a class of old passively evolving objects (old-EROs) with derived minimum age of ~ 3 Gyr, corresponding to a formation redshift of $z_f \gtrsim 2.4$. Pure luminosity evolution models with such formation redshifts well reproduce the density of old EROs (consistent with being passively evolving ellipticals), whereas the predictions of the current hierarchical merging models are lower than the observed densities by large factors (up to an order of magnitude). In this survey, a population of dusty star-forming galaxies is also identified at $0.7 < z < 1.5$, equally populated as the old-EROs ensemble, and suggests a significant contribution to the cosmic star-formation density at $z_f \sim 1$.

On the theoretical side, Chiosi & Carraro (2002) nicely summarized the current situation by highlighting that the hierarchical scheme melting together subunits made of gas and stars is not the dominant one by which elliptical galaxies are made unless it has taken place in the very remote past.

Independent of the adopted scenario for the formation and evolution of elliptical galaxies, models should meet some observational constraints on the history of star-formation of these objects. These constraints include ages, metallicities and degree of enhancement in α-elements, derived by means of line-strength indices and Single Stellar Population (SSP) models (e.g., González 1993; Worthey 1994; Kuntschner 2000, 2001; Trager *et al.* 2000a; T00b; Thomas, Maraston & Bender 2003, hereafter TMB03; Thomas, Maraston & Korn 2004).

This paper explores the central stellar populations of a sample of local early-type galaxies and search for correlations among them and with structural parameters. Many previous works have studied such correlations (e.g. Tantalo, Chiosi & Bressan 1998; Jørgensen 1999; Trager *et al.* 2000a; T00b; Kuntschner 2000; Terlevich & Forbes 2002). We pay special attention to T00b, as many of the analysis presented here were first explored by these authors. We would like to highlight the high mean signal-to-noise of our sample and the use of the TMB03 set of SSP models for the analysis in this paper. TMB03 presented an empirical calibration for the synthetic Lick indices of SSP models that for the first time extended up to solar metallicity. The new metallicity range covered approaches the regime that is relevant for the interpretation of the integrated spectra of elliptical galaxies.

In Section 2 we briefly describe the sample and stellar population model applied. In Section 3 we explore the line-strength Lick indices and the quality of the model calibrations. The determination of ages and metallicities, and the enhanced-element ratio [α/Fe] are presented in Sections 4 and 5, respectively. We investigate the existence of the age-metallicity-σ_0-[α/Fe] hyperplane for early-type galaxies in Section 6. Discussions and conclusions from the nuclear stellar population analysis are presented in Sections 7 and 8. Finally, in Section 9 we explore our large spectral coverage to compare metallicities derived from different elements, in the form of a log(O/H) *vs* [Z/H] plot.

2 DATA AND ADOPTED MODEL

In the present work we will be analysing the spectra for 83 galaxies with signal-to-noise (S/N) ratio greater than 15 (per resolution element FWHM = 6 Å) for the $r_e/8$ central aperture extraction. The observations were performed at the 2.12 m telescope of the *Observatorio Astrofísico Guillermo Haro* (OAGH), at Cananea, Mexico. Eight galaxies in our sample were carefully classified as isolated (typical Tully 1987 density of 0.08); the sample also has 18 galaxies in the field, and 57 group members. The group classification is taken from Garcia (1993). The sample also contains three Virgo cluster galaxies, namely NGC 4365, NGC 4374, NGC 4754, with the respective Tully (1987) catalogue density of 2.93, 3.99 and 2.62. In total, the sample consists of 52 elliptical galaxies and 31 bulges of S0s or early-type spirals. Note the original sample had 86 galaxies, but for the present analysis the galaxies NGC 3139, NGC 5854 and NGC 5869 were not used because they do not have spectral information at $\lambda \lesssim$ 5100 Å, and so no ages and metallicities could be derived. Therefore, the total sample with age and [Z/H] information has 83 galaxies. The full details of the sample, observations, data reduction and index measurements are presented in Denicoló *et al.* (2004, hereafter Paper I).

The spectra cover a wavelength range from $\sim$ 3850 Å to $\sim$ 6700 Å. The median S/N of the sample is 40 per resolution element. The Lick/IDS line-strength index measurements were performed separately in each galaxy frame and later averaged, the error of the mean was computed from the repeated measurements per galaxy (on average, there are 8 spectral frames per galaxy).

Kinematic information for the galaxies was carefully derived in Paper I. 25 Lick spectral indices were measured and calibrated to the Lick/IDS system. Most of the galaxies in the sample had the Balmer indices corrected for emission using Hα detection. The emission correction with Hα should be less uncertain than the empirical emission correction of the Balmer lines using [O III] λ5007 Å.

In this work we refer to our sample as the OAGH sample, and use the following definitions for the special spectral indices: <Fe> = (Fe4383+Fe5270+Fe5335)/3 and [MgFe] = $[Mgb \cdot (0.72 \cdot Fe5270 + 0.28 \cdot Fe5335)]^{1/2}$, as in Kuntschner (1998) and TMB03, respectively.

TMB03 have constructed stellar population models for various and well-defined element abundance ratios. The most important ratio is α/Fe, which is the ratio of the so-called α-elements (O, Ne, Mg, Si, S, Ar, Ca) to the Fe-peak

elements (Cr, Mn, Fe, Co, Ni, Cu, Zn), because it carries information on the formation time-scale of stellar populations. The whole set of Lick indices of SSP models is presented with [α/Fe] ratios of 0.0, 0.3, 0.5. The impact from the element abundance changes on the absorption-line indices are taken from Tripicco & Bell (1995, TB95), using an extension of the method introduced by T00b. The models are calibrated with the globular cluster data of Puzia *et al.* (2002). The present models now allow for the unambiguous derivation of SSP ages, metallicities, and element abundance ratios, in particular [α/Fe] ratios. For this reason we have adopted their models throughout this paper. We note that recent results from the same group of authors (Thomas, Maraston & Korn 2004) have extended the models of variable abundance ratios to the Balmer lines. The key result is that, unlike Hβ, the Hδ and Hγ indices show a marked dependence on [α/Fe] ratio. We will discuss this dependence again in the next Section.

3 EXPLORING NUCLEAR LINE-STRENGTH INDICES

There are considerable shifts in metallicity and age when comparing TMB03 models with G. Worthey's SSP models (W94). Figure 1 presents a comparison between model tracks for the same age and [Fe/H] grid steps. Taking the position of the galaxy NGC 3379 in the diagram, we have interpolated an age of 10.9 $\pm^{2.6}_{2.8}$ Gyr and [Fe/H] = 0.30 $\pm^{0.07}_{0.08}$ dex using TMB03 models, while W94 models result in 11.4 $\pm^{3.9}_{2.6}$ Gyr and [Fe/H] = 0.22 $\pm^{0.07}_{0.08}$ dex. The ages and metallicities were interpolated as will be explained in Section 4.

The metallicity values derived from interpolation of the TMB03 model are generally higher than with the W94 model (in the case of NGC 3379, TMB03 results +0.08 dex higher in metallicity than W94). Likewise, the ages are systematically younger in TMB03 by comparison with W94.

We note that the emission correction (see Paper I, Section 4) used in this work is, in general, larger than in previous works. The effect of a higher emission correction, i.e., a higher Hβ value, is a decrease in age and consequent increase in metallicity, due to the bending of the model tracks. Hence, one should keep in mind that both the use of new model tracks and the larger emission correction are responsible for differences in age/metallicity values when comparing with the literature.

Note however, that the differences between the age and [Fe/H] from W94 and TMB03 models for NGC 3379 are not representative of the uncertainties involved in these determinations. The uncertainty in the age and [Fe/H] values for NGC 3379 is of greater magnitude than the difference between the models. We will discuss the errors in age and metallicity determinations in Section 4.1.

3.1 Model vs data

The aim of the initial paragraphs of this section is to decide which combination of indices provides a reliable and well-understood determination of the stellar population age and metallicity. For that, and to assess the consistency of our index measurements in relation to the model predictions we present index-index plots which are almost degenerate in age and metallicity. We separate the indices in three groups based upon their sensitivity to α elements, Fe-peak elements, and the Balmer lines. This group distinction is also useful to check how well the various Lick indices trace the corresponding element abundance. An analysis of the same type was carried out by TMB03, and we feel it is important to show the consistency of the models with respect to our sample as well. In the following figures we plot 83 galaxies observed at OAGH.

We analyse firstly the Balmer-line indices. Figure 2

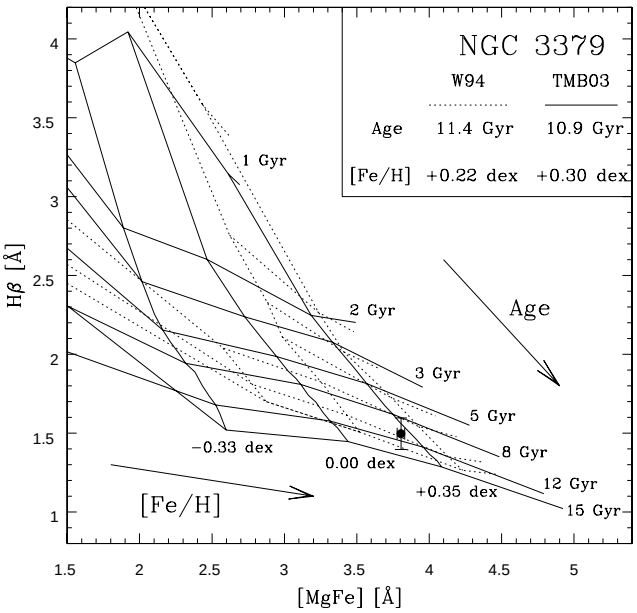

Figure 1. Comparison between Worthey (1994, W94) and Thomas, Maraston & Bender (2003, TMB03) models. Both models are shown in age steps of 1, 2, 3, 5, 8, 12, 15 Gyr and metallicity steps of -0.33, 0.00, +0.35. The Worthey model was interpolated to the given age and metallicity steps with the use of G. Worthey's home page (http://astro.wsu.edu/∼worthey/). The point represents NGC 3379.

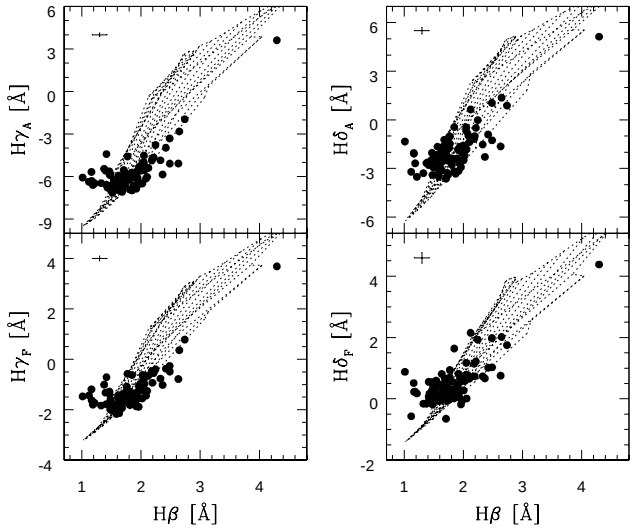

Figure 2. Index *vs* index plots for Balmer-line indices in the Lick/IDS system. Overplotted are the model predictions by TMB03. The solid circles are 83 galaxies from our sample. The error bars represent the average error of the mean per index, from repeated observations.

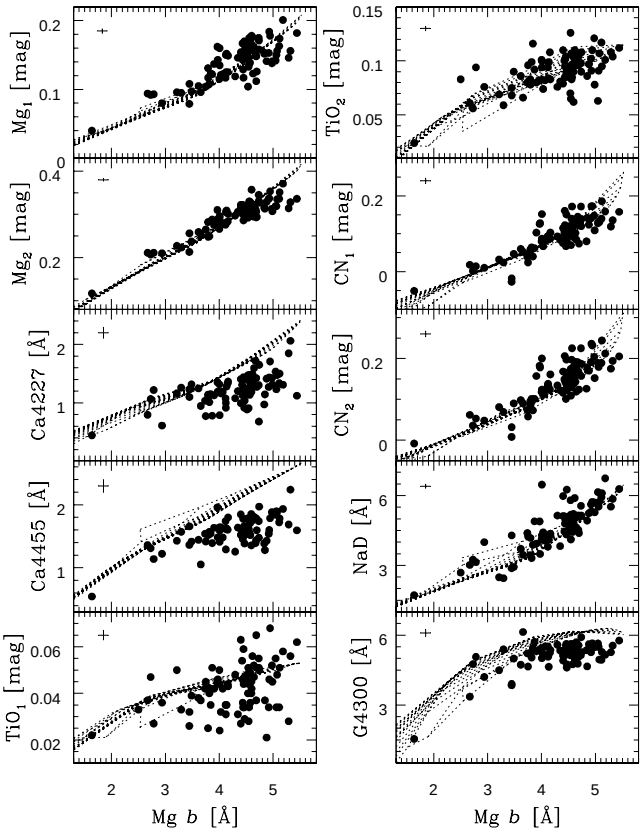

Figure 3. Index *vs* index plots for indices that correlate with Mg. The symbols are the same as in Figure 2.

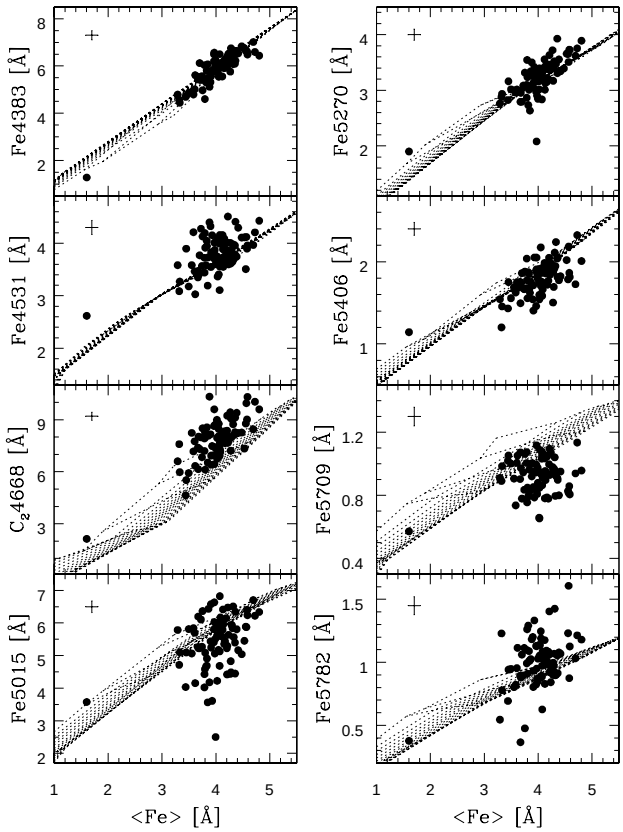

Figure 4. Index *vs* index plots for Fe-peak indices. The symbols are the same as in Figure 2.

shows the relation between Hβ, H$\gamma_{A,F}$ and H$\delta_{A,F}$. The Hβ index is only marginally affected by the [α/Fe] ratio, as discussed in TB95 and in Thomas *et al.* (2004), i.e., more important for the modelling is taking correct account of the Horizontal Branch morphology (Maraston *et al.* 2003). The models used here have the mass-loss on the red giant branch phase taken into account, as calibrated in Maraston & Thomas (2000). The agreement between models and observations is not as good as one would expect, even given the observational errors. However, Thomas *et al.* (2004) discuss about the important dependence of the higher order Balmer lines H$_{\delta,\gamma}$ on [α/Fe]. To correctly compare the Balmer lines then we would need to previously know the overabundance ratio for each galaxy and use the corresponding model grid for each galaxy [α/Fe] value. This fact certainly diminishes the advantage of higher-order Balmer line indices over Hβ as age indicators, as we will discuss in Section 4. We then emphasize to the reader that some mismatch between galaxies and models of higher-order Balmer lines at constant [α/Fe] is expected, because H$_{\delta,\gamma}$ change significantly for different [α/Fe] ratios.

In Figure 3 the α-element sensitive indices Mg$_{1,2}$, TiO$_{1,2}$, NaD, CN$_{1,2}$ seem consistent with each other. The "Ca lines", Ca4227 and Ca4455, show a mismatch with the models; this mismatch grows with increasing Mg*b*. Indeed the model predictions of the Ca4227 index seem to be slightly too high as discussed in Maraston *et al.* (2003); those authors indicate that models with variable α/Ca could explain the difference.

We have plotted the Ca4455 index in the same diagram of the α-element sensitive indices to exemplify how misleading can be the actual index nomenclature. Despite its name Ca4455 is insensitive to Ca abundance (TB95), while Fe and Cr, both elements of the "depressed" group, are the dominant contributors to this index. Concerning the model tracks, Ca4455 responds strongly to [α/Fe] ratio, and it most likely suffers from calibration problems (Maraston *et al.* 2003).

The TiO$_2$ agrees reasonably well with Mg*b* at different metallicities. NaD also behaves consistently with Mg*b*, but the high sensitivity of the NaD index to interstellar absorption severely hampers its usefulness for stellar population studies (Worthey *et al.* 1994). We noticed that probably part of the scatter in the TiO$_1$ index is due to the broad NaD feature, once the blue pseudocontinuum of TiO$_1$ is very close in wavelength to the NaD profile. The CN indices show a good match between the galaxy sample and the models. We observe a mismatch of models and galaxy data for the G4300 index. The calibration of the models with the globular cluster data for this index is also not convincing as already noted by Puzia *et al.* (2002).

In the diagrams with the indices most sensitive to Fe (Figure 4), we draw attention to the relatively large scatter in the index values for Fe5709, Fe5782, and specially for Fe5015, the last one mainly due to uncertainties in the emission contamination correction (the index Fe5015 was emission corrected as explained in Paper I, Section 4.2.2). We plotted the C$_2$4668 index together with the Fe group as in

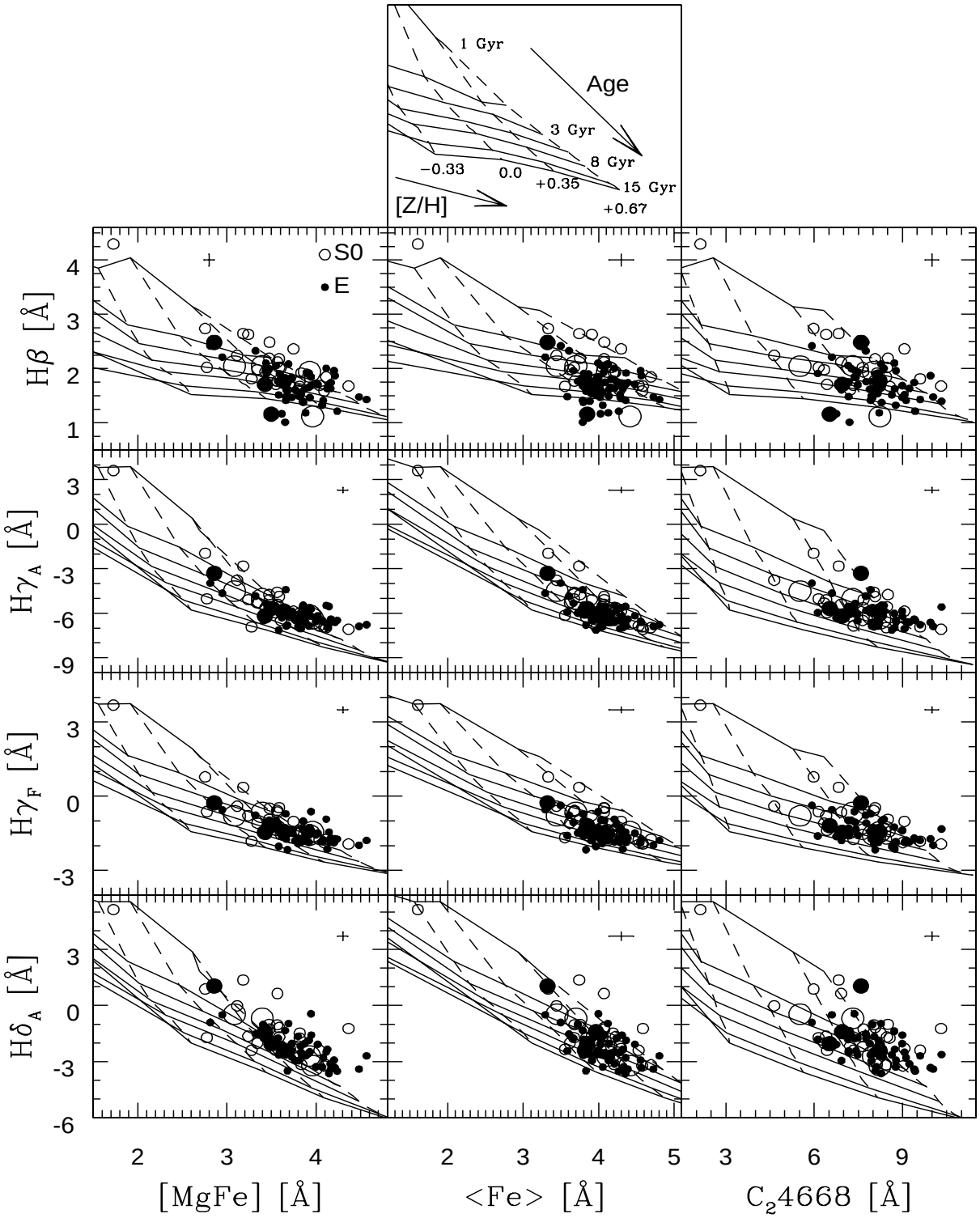

Figure 5. Age-metallicity diagnostic diagrams. The Balmer-line indices are corrected for nebular emission as explained in Paper I. Overplotted are the model predictions by TMB03 (with [α/Fe] = 0.0). The dashed lines represent lines of constant metallicity ([Z/H] = -1.35, -0.33, 0.00, +0.35, +0.67 dex), whereas the solid lines are lines of constant age (ages = 1, 2, 3, 5, 8, 12 and 15 Gyr). Open symbols denote S0 galaxies, solid symbols represent elliptical galaxies. Isolated galaxies are plotted with larger symbols. The error bars at the top of the plots are the average error of the mean per index. The left-top corner S0 galaxy far away from the main distribution of galaxies is NGC 3156.

Maraston *et al.* (2003). Although this index is supposed to follow carbon, it shows a correlation with Fe. $C_2$4668 must have calibration problems too and its mismatch with the models cannot be explained by overabundance (TMB03). As in the globular clusters studies, this index shows a poor match between models and data (Puzia *et al.* 2002). In view of modelling uncertainties (TMB03; the mismatch of $C_2$4668 between model and observation cannot be explained only by α/Fe effects), $C_2$4668 becomes an index not well suited for element abundance studies.

In all, the distribution of the OAGH galaxies in these diagrams is very similar to the distribution of the bulk of galaxies from the sample of 381 Lick/IDS galaxies in Trager *et al.* (1998) (see comparison of data and models in TMB03).

As pointed out by Worthey (1994) the determination of the age of old stellar populations is complicated by the similar effects that age and metallicity have on the integrated spectral energy distributions. Broad band colours and most of the indices are degenerate along the locus of Δ age $\approx$ -3/2 Δ Z. Worthey dubbed this behaviour the "3/2 rule". In other words, the integrated SED of an old ($\gtrsim$ 2 Gyr) stellar population looks almost identical when age is doubled and Z reduced by a factor of three at the same time. Only a few narrow band weak absorption line indices have so far been identified which can potentially break this degeneracy. In terms of age, the Balmer lines Hβ, Hγ and Hδ are the most promising features, being clearly more sensitive to age than to metallicity. Features which are more metal sensitive, and thus less age sensitive than the average are: $C_2$4668, Mg_2, Fe5270, Fe5335 and Fe4383.

In Figure 5 we show metallicity *vs* age indicators, in the form of [MgFe], <Fe>, $C_2$4668 against Hβ, H$\gamma_{A,F}$ and Hδ_A. Note that the degeneracy of the models is stronger for older metal rich systems, i.e. those in the bottom right corner of the diagrams. Both ellipticals and S0s show a spread in age of a factor of about 4 (mostly between 3-12 Gyr), and a larger spread in metallicities (approximately from -0.33 to +0.67 dex). The outlier galaxy on the top-left corner of the plots in Figure 5 is NGC 3156, a disk-dominated S0 galaxy with a rather faint bulge (Michard & Marchal 1994). As we have seen, when well calibrated by the models, $C_2$4668 could be the most promising index for [Fe/H] determinations given its high sensitivity to metallicity (its range of variation from [Z/H] solar to three times solar is about 5 Å). Considering ease of measurement, existing calibrations, large metallicity dependence, small age dependence, and relatively tight relation, we can say that, at present, the best metallicity indicator in Figure 5 is [MgFe]. Note that we are using the [MgFe] index defined in TMB03, where Fe5270 and Fe5335 are weighted as 72% and 28%, respectively, to balance the [α/Fe] dependence (see Fig.7 of TMB03).

Concerning age indicators, Hβ is still the best calibrated Balmer-line index, even though it suffers from emission contamination. The higher order Balmer lines (i.e., Hγ, Hδ) are a lot less sensitive to emission (see Table 6 in Paper I), but at the same time they are more affected by abundance effects because of the presence of more metallic lines in the bluer parts of the spectrum (Thomas *et al.* 2004). Maraston *et al.* (2003) present a calibration of the Balmer lines, in $H_{\beta,\gamma,\delta}$ *vs* [MgFe] diagrams, for 12 globular clusters with [MgFe] $\lesssim$ 3.5 Å. We emphasize that, as in TMB03 (their Fig.2, concerning index calibration) the behaviour of globular clusters does not always represent the range of values covered by galaxies. There are significant differences in the index calibration for clusters and galaxies specially for indices such as $C_2$4668, $CN_{1,2}$, Ca4227, Ca4455, NaD, $TiO_{1,2}$, Hδ and Hγ. The Hβ-index calibration for globular clusters seems robust, despite the very large scatter of the galaxy sample from Trager *et al.* (1998).

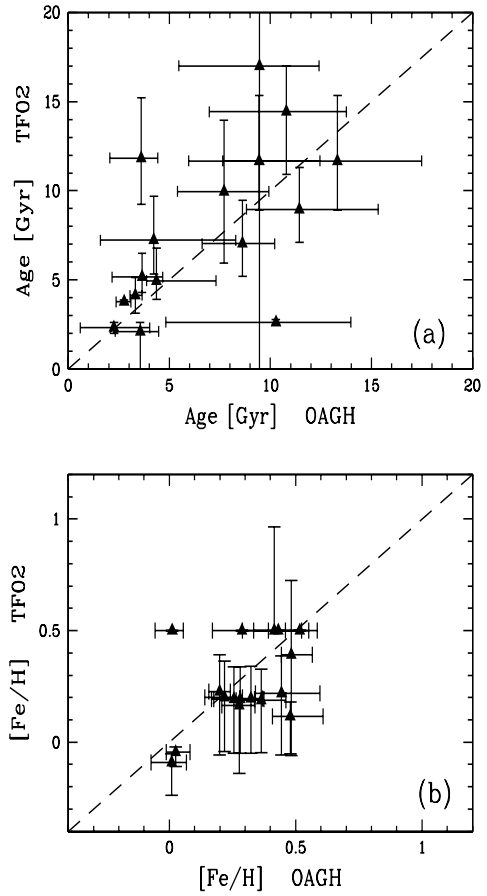

Figure 6. The panels compare the ages and metallicities in the catalogue by Terlevich & Forbes (2002, TF02) with our data determinations (OAGH). One-to-one correspondence is indicated by the dashed line. We have interpolated ages and metallicities for 15 galaxies in common with TF02. Both age and metallicity values for this comparison were derived from the Hβ *vs* [MgFe] diagram, using Worthey (1994) stellar population models (see Table 1).

In this work, ages and metallicities (according to the TMB03 models) are derived from the [MgFe] *vs* Hβ plane as shown in Figure 5 (and also in the top panel of Figure 7). Note that there is some level of mismatch between data and models and a significant number of galaxies falls outside the models. We interpolated between the model grid points, but did not attempt to extrapolate to ages or metallicities greater than 15 Gyr or 0.67 dex, respectively (in the plots we have denoted these galaxies by arrows and placed them with symbolic values for age: 16 Gyr and [Z/H]: 0.69 dex). The only galaxy we attempted to extrapolate a consistent age and [Z/H] value was NGC 3156. We have used a polynomial interpolation of varying order, depending on the position

Table 1. Comparison with TF02 of ages and metallicities derived using Worthey (1994) models.

Galaxy	Age OAGH [Gyr]	Age TF02 [Gyr]	[Fe/H] OAGH [dex]	[Fe/H] TF02 [dex]
NGC 221	$2.8^{+0.3}_{-0.4}$	$3.8^{+0.1}_{-0.1}$	$0.03^{+0.06}_{-0.04}$	$-0.04^{+0.06}_{-0.02}$
NGC 584	$3.6^{+0.9}_{-1.2}$	$2.1^{+0.5}_{-2.1}$	$0.42^{+0.11}_{-0.08}$	$0.50^{+0.46}_{-0.0}$
NGC 821	$4.2^{+4.0}_{-2.6}$	$7.2^{+2.5}_{-1.9}$	$0.44^{+0.15}_{-0.10}$	$0.22^{+0.17}_{-0.28}$
NGC 1700	$2.3^{+1.8}_{-1.6}$	$2.3^{+0.3}_{-0.3}$	$0.43^{+0.15}_{-0.14}$	$0.50^{+0.00}_{-0.00}$
NGC 2300	$4.4^{+2.9}_{-0.5}$	$5.0^{+1.8}_{-1.1}$	$0.48^{+0.08}_{-0.04}$	$0.39^{+0.33}_{-0.45}$
NGC 3377	$3.3^{+0.3}_{-0.3}$	$4.1^{+1.0}_{-1.0}$	$0.32^{+0.05}_{-0.04}$	$0.20^{+0.14}_{-0.24}$
NGC 3379	$11.4^{+3.9}_{-2.6}$	$9.0^{+2.3}_{-1.9}$	$0.22^{+0.07}_{-0.08}$	$0.20^{+0.16}_{-0.24}$
NGC 3608	$7.7^{+2.2}_{-2.3}$	$10.0^{+4.0}_{-4.0}$	$0.28^{+0.06}_{-0.07}$	$0.16^{+0.02}_{-0.30}$
NGC 4261	$10.8^{+3.0}_{-3.8}$	$14.4^{+2.6}_{-3.5}$	$0.36^{+0.10}_{-0.10}$	$0.19^{+0.14}_{-0.23}$
NGC 4374	$3.6^{+0.8}_{-1.6}$	$11.8^{+3.4}_{-2.6}$	$0.48^{+0.13}_{-0.07}$	$0.12^{+0.06}_{-0.17}$
NGC 5638	$8.6^{+1.6}_{-2.0}$	$7.0^{+2.4}_{-1.8}$	$0.20^{+0.04}_{-0.04}$	$0.23^{+0.17}_{-0.28}$
NGC 5831	$10.3^{+3.7}_{-5.4}$	$2.6^{+0.2}_{-0.2}$	$0.29^{+0.10}_{-0.12}$	$0.50^{+0.00}_{-0.00}$
NGC 5846	$9.4^{+3.0}_{-3.5}$	$11.7^{+3.7}_{-2.7}$	$0.26^{+0.08}_{-0.09}$	$0.19^{+0.14}_{-0.24}$
NGC 7454	$3.6^{+1.0}_{-1.5}$	$5.2^{+1.3}_{-0.9}$	$0.01^{+0.06}_{-0.08}$	$-0.09^{+0.15}_{-0.04}$
NGC 7626	$13.3^{+4.2}_{-5.7}$	$11.7^{+3.6}_{-2.7}$	$0.28^{+0.09}_{-0.10}$	$0.19^{+0.14}_{-0.24}$

of the galaxy in the [MgFe] *vs* Hβ diagram. For instance, galaxies placed in the region of 1-3 Gyr have less neighbouring model points (i.e., lower order) than galaxies older than 8 Gyr (more neighbouring data points = higher order interpolation). This is because, as we have stated before, the degeneracy of the models is stronger for older systems. Every determination of age and metallicity was double-checked against the location in the [MgFe] *vs* Hβ plane for consistency of the results. We should always bear in mind that non-linear interpolations using distant spaced model points as in the case of TMB03 model grids, may result in non-stable determinations and there is always the possibility of wild oscillations between the tabulated points (see discussion about interpolation algorithms in Press *et al.* 1992).

It is important to notice that the *ages and metallicities derived here should not be taken as absolute values*; there are systematic offsets if different index combinations are used, although the relative ranking of the galaxies in the sample should not be very different (cf. Figure 5). In the TMB03 system, the average age for the group, field and isolated sample (excluding the three Virgo cluster galaxies) is 4.2 Gyr, with an average metallicity of +0.41 dex. The cluster galaxies in our sample also present rather young ages (NGC 4365: 3.6 Gyr, NGC 4374: 3.8 Gyr, NGC 4754: 5.8 Gyr). Both elliptical and S0 galaxies in our sample show similar spread in age and metallicity in the [MgFe]-Hβ diagram with a marginal tendency for the bulge of S0s to be slightly younger than the elliptical galaxies, as will be shown in Section 4.

In panels *a* and *b* of Figure 6 we compare our determinations with ages and metallicities in the Terlevich & Forbes (2002, TF02) catalogue, for which the authors have compiled ages, metallicities and abundances from the highest quality data of early-type galaxies in the literature. In TF02, ages and [Fe/H] were derived by interpolating Worthey (1994, W94) stellar population models in the Hβ-[MgFe] plane. To carry out this comparison, we have also interpolated ages and metallicities using W94 models.

Figure 6 shows a reasonably good agreement, inside the errors, between 15 galaxies in common with TF02 (see also Table 1). Our ages are in general slightly younger most probably due to the emission correction applied in this work. Panel *b* reveals the corresponding small shift to higher metallicities also very likely caused by the higher Hβ values resulting after the emission correction. There is indeed a correlation between Δ age (TF02-OAGH) and the applied emission correction EC(Hβ) (Paper I).

4 AGES AND METALLICITIES

The [Z/H] – log *Age* relation is presented in the bottom panel of Figure 7. The small arrows represent lower limits in age and metallicity for the galaxies that fall outside the model grids. Those galaxies for which we can only give a lower limit in age are mostly ellipticals, while those for which we give a lower limit in metallicity are as many ellipticals as S0s. It is worth emphasizing that the age and metallicity values derived are not absolute, only the ranking of the galaxies is relatively independent of the adopted models. An error ellipse is shown at the bottom corner of the plot. This 1σ error ellipse is the result of the interpolation in the Hβ-[MgFe] plane of a galaxy with Hβ error of 0.11 Å and [MgFe] error of 0.06 Å, which correspond to the mean error values for these indices in the sample. Note that the correlation between age and [Z/H] in Figure 7 (roughly Δ log *age* $\cong -1.57\ \Delta$ [Z/H]) is consistent with being originated by correlated errors, as the spread of points has similar orientation to the major-axis of the error "ellipse". A Spearman correlation test results in ρ = -0.566 with more than 90% probability that a correlation is present. The vectors shown in the error ellipse correspond to 0.078 dex in [Z/H] and 0.17 dex in log Age; these values are a rough average of the overall uncertainties in age and metallicity determinations for our sample. A further analysis of the errors in the age-metallicity diagram is presented in the next Section.

S0s and Es show a slightly different distribution in the plane [Z/H] *vs* log *Age*. Excluding the three Virgo cluster galaxies, the sample of mostly low-density environment galaxies is composed of 50 ellipticals and 30 S0s. The median age value for Es is 5.8 $\pm$ 0.6 Gyr, and for S0s is 3.0 $\pm$ 0.6 Gyr, where the uncertainties are the errors of the mean. The median metallicity value for Es is 0.37 $\pm$ 0.03 dex and for S0s, 0.53 $\pm$ 0.04 dex. Therefore S0 galaxies seem to be slightly younger and more metal-rich than ellipticals. However the elliptical galaxies in our sample show a larger spread in age distribution than S0s. Note also that the metallicities of the young S0 galaxies are subject to large errors because they are likely to have disk contamination, i.e., composite stellar populations. In particular, the isolated galaxies themselves also cover a large range in metallicity *and* age. On the other hand, our two Virgo cluster elliptical galaxies are placed relatively close to each other in age (filled square symbols in Figure 7). It might be expected that cluster galaxies constitute a more homogeneous sample (as demonstrated in the Fornax cluster by Kuntschner 1998), with perhaps a larger spread in metallicities than in ages. Table 2 presents the ages and [Z/H] values for our sample.

It is important to note that the age/metallicity analysis presented here depends on the assumption of a single (luminosity weighted) stellar population, which we feel is a reasonable one. The presence of additional populations (especially if they are luminous) will bias – perhaps signifi-

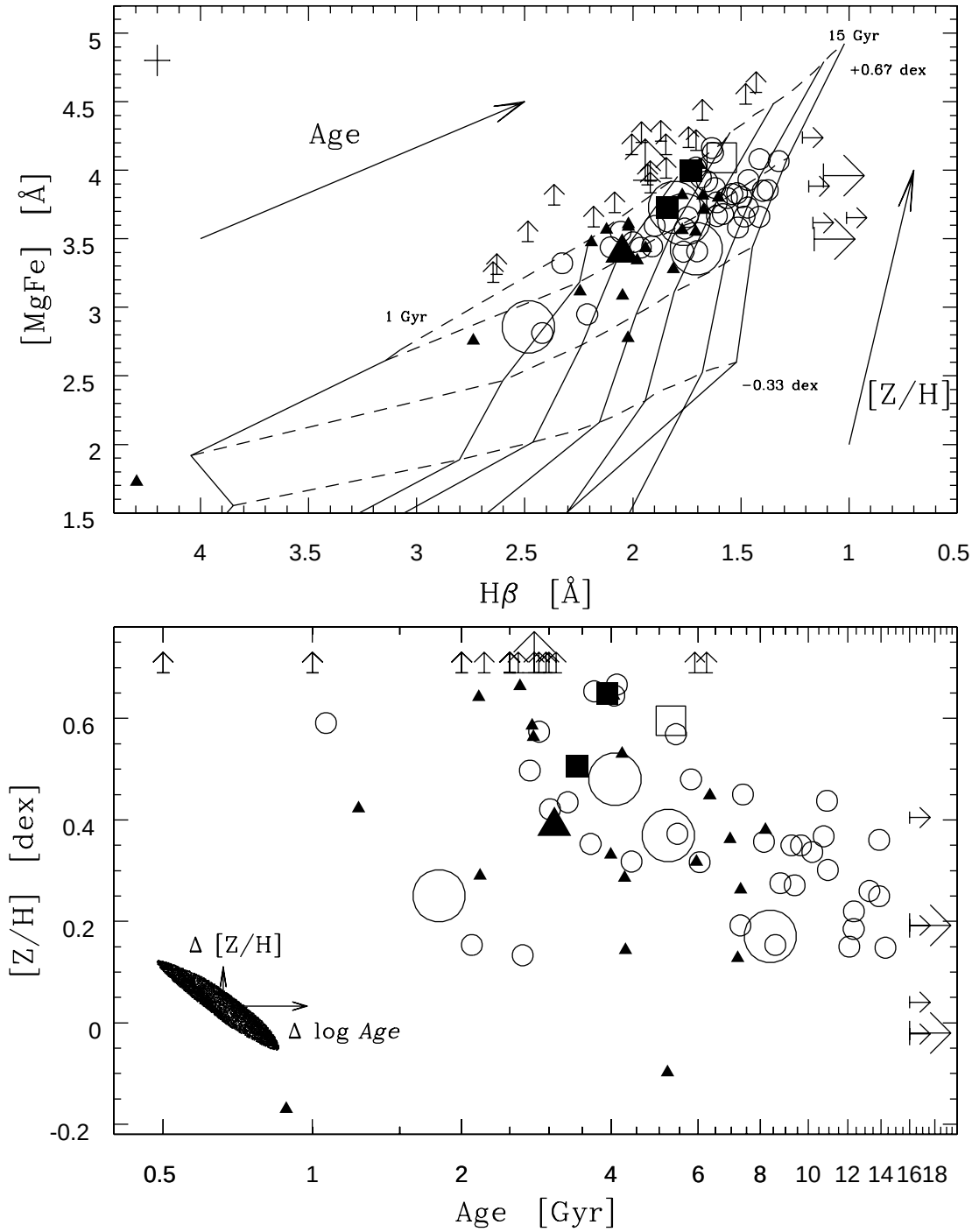

Figure 7. The top panel shows the Hβ-[MgFe] plane from where Age and [Z/H] were interpolated using the TMB03 model grids. The model grids are shown in age steps of 1, 2, 3, 5, 8, 12, 15 Gyr and metallicity steps of -0.33, 0.00, +0.35, +0.67 dex. The derived age *vs* [Z/H] diagram is shown in the bottom panel. Open circles represent elliptical galaxies and filled triangles are S0-type galaxies in the sample. Large circles and the large triangle are isolated galaxies. The three Virgo cluster galaxies in the sample, NGC 4365, NGC 4374, NGC 4754, are plotted as square symbols (S0 is open square, Es are filled squares). The average 1σ error ellipse is presented at the bottom left corner of the age *vs* [Z/H] diagram. The vectors shown in the error ellipse correspond to 0.078 dex in [Z/H] and 0.17 in log Age.

Table 2. Age, [Z/H] and [α/Fe] from nuclear $r_e/8$ extractions.

Galaxy	Age [Gyr]	[Z/H] [dex]	[α/Fe]† [dex]	Galaxy	Age [Gyr]	[Z/H] [dex]	[α/Fe]† [dex]
ESO462-G015	$5.6^{+1.0}_{-2.0}$	$0.37^{+0.17}_{-0.20}$	0.24	NGC 3414	$6.0^{+3.0}_{-3.7}$	$0.43^{+0.09}_{-0.13}$	0.34
MCG-01-03-018	$>^{+1.2}_{-3.6}$	$0.19^{+0.06}_{-0.06}$	0.09	NGC 3599	$1.2^{+0.1}_{-0.4}$	$0.30^{+0.15}_{-0.14}$	-0.04
NGC 0016	$2.8^{+0.05}_{-0.1}$	$0.56^{+0.04}_{-0.05}$	0.10	NGC 3607	$2.7^{+1.0}_{-0.7}$	$0.67>^{+0.12}_{-0.07}$	0.17
NGC 0221	$2.1^{+0.2}_{-0.2}$	$0.15^{+0.04}_{-0.05}$	-0.10	**NGC 3608**	$8.1^{+2.8}_{-3.1}$	$0.36^{+0.04}_{-0.17}$	0.27
NGC 0315	$2.5^{+1.0}_{-1.0}$	$>^{+0.37}_{-0.02}$	0.20	**NGC 3610**	$1.8^{+0.2}_{-0.5}$	$0.59^{+0.21}_{-0.18}$	0.12
NGC 0474	$7.3^{+2.0}_{-2.4}$	$0.26^{+0.07}_{-0.07}$	0.09	**NGC 3613**	$5.6^{+1.7}_{-2.5}$	$0.37^{+0.07}_{-0.07}$	0.10
NGC 0584	$3.8^{+0.5}_{-1.7}$	$0.43^{+0.07}_{-0.10}$	0.15	**NGC 3636**	$4.4^{+1.4}_{-2.0}$	$0.32^{+0.09}_{-0.10}$	0.08
NGC 0720	$3.0^{+0.5}_{-4.3}$	$>^{+0.12}_{-0.02}$	0.23	**NGC 3640**	$2.5^{+0.7}_{-0.3}$	$0.53^{+0.13}_{-0.13}$	0.12
NGC 0750	$14.0^{+3.4}_{-1.7}$	$0.25^{+0.04}_{-0.10}$	0.23	NGC 3665	$2.0^{+1.0}_{-0.8}$	$>^{+0.08}_{-0.07}$	0.16
NGC 0751	$8.6^{+1.9}_{-2.4}$	$0.15^{+0.08}_{-0.08}$	0.03	**NGC 3923**	$2.6^{+0.5}_{-0.6}$	$>^{+0.04}_{-0.07}$	0.14
NGC 0777	$13.3^{+6.7}_{-5.2}$	$0.26^{+0.20}_{-0.20}$	0.26	NGC 3941	$2.6^{+0.4}_{-0.3}$	$0.55^{+0.13}_{-0.12}$	0.07
NGC 0821	$4.0^{+1.7}_{-3.5}$	$0.48^{+0.13}_{-0.17}$	0.17	**NGC 4125**	$5.9^{+2.5}_{-3.0}$	$0.32^{+0.10}_{-0.10}$	0.10
NGC 0890	$2.2^{+0.4}_{-0.4}$	$0.60^{+0.08}_{-0.07}$	0.12	**NGC 4261**	$10.6^{+4.7}_{-4.7}$	$0.44^{+0.10}_{-0.03}$	0.22
NGC 1045	$2.6^{+0.8}_{-2.7}$	$>^{+0.14}_{-0.06}$	0.14	**NGC 4365**	$3.6^{+3.7}_{-2.3}$	$0.65^{+0.10}_{-0.06}$	0.20
NGC 1052	$2.9^{+0.4}_{-8.8}$	$>^{+0.34}_{-0.03}$	0.34	**NGC 4374**	$3.8^{+1.1}_{-2.7}$	$0.50^{+0.11}_{-0.15}$	0.23
NGC 1132	$>^{+5.1}_{-14.9}$	$-0.02^{+0.19}_{-0.16}$	0.24	**NGC 4494**	$6.7^{+0.4}_{-0.3}$	$0.19^{+0.04}_{-0.04}$	0.17
NGC 1407	$2.5^{+0.5}_{-0.8}$	$>^{+0.01}_{-0.09}$	0.18	NGC 4550	$2.3^{+1.4}_{-4.4}$	$0.29^{+0.25}_{-0.40}$	0.05
NGC 1453	$>^{+4.7}_{-1.7}$	$0.45^{+0.04}_{-0.09}$	0.19	NGC 4754	$5.8^{+1.9}_{-2.5}$	$0.55^{+0.07}_{-0.08}$	0.15
NGC 1600	$2.7^{+0.5}_{-1.0}$	$>^{+0.00}_{-0.06}$	0.13	**NGC 5322**	$2.4^{+0.4}_{-0.4}$	$>^{+0.09}_{-0.06}$	0.14
NGC 1700	$2.6^{+1.4}_{-1.8}$	$0.45^{+0.19}_{-0.21}$	0.11	NGC 5353	$3.0^{+0.3}_{-1.7}$	$>^{+0.02}_{-0.03}$	0.21
NGC 1726	$7.0^{+4.0}_{-5.4}$	$0.36^{+0.07}_{-0.16}$	0.34	**NGC 5354** 90^o	$>^{+0.9}_{-7.3}$	$0.00^{+0.09}_{-0.05}$	0.14
NGC 2128	$3.1^{+2.6}_{-5.4}$	$0.39^{+0.16}_{-0.36}$	0.30	**NGC 5354** 0^o	$9.3^{+3.6}_{-3.9}$	$0.34^{+0.13}_{-0.06}$	0.14
NGC 2300	$4.0^{+1.2}_{-1.4}$	$0.53^{+0.05}_{-0.06}$	0.19	NGC 5363	$3.8^{+2.1}_{-3.5}$	$0.29^{+0.11}_{-0.19}$	0.24
NGC 2418	$4.8^{+2.6}_{-2.8}$	$0.57^{+0.12}_{-0.11}$	0.16	**NGC 5444**	$>^{+0.5}_{-3.4}$	$0.17^{+0.05}_{-0.03}$	0.25
NGC 2513	$3.8^{+2.4}_{-2.0}$	$^{+0.07}_{-0.08}$	0.22	**NGC 5557**	$7.0^{+1.3}_{-1.4}$	$0.45^{+0.07}_{-0.07}$	0.18
NGC 2549	$1.5^{+0.3}_{-0.5}$	$>^{+0.01}_{-0.20}$	0.05	**NGC 5576**	$3.2^{+0.2}_{-1.2}$	$0.42^{+0.08}_{-0.11}$	0.07
NGC 2768 0^o	$8.0^{+3.5}_{-3.8}$	$0.38^{+0.29}_{-0.20}$	0.12	**NGC 5638**	$8.8^{+1.4}_{-1.5}$	$0.28^{+0.05}_{-0.05}$	0.21
NGC 2768 90^o	$3.8^{+1.0}_{-1.3}$	$0.64^{+0.06}_{-0.03}$	0.12	**NGC 5812**	$3.8^{+0.8}_{-1.6}$	$0.65^{+0.15}_{-0.03}$	0.21
NGC 2872	$9.7^{+4.7}_{-5.9}$	$0.35^{+0.14}_{-0.16}$	0.27	**NGC 5813**	$9.8^{+3.3}_{-3.8}$	$0.27^{+0.10}_{-0.10}$	0.25
NGC 2911	$2.4^{+1.6}_{-1.7}$	$0.66^{+0.29}_{-0.05}$	0.20	**NGC 5831**	$10.7^{+3.5}_{-4.6}$	$0.37^{+0.10}_{-0.12}$	0.18
NGC 2974	$14.3^{+3.6}_{-1.5}$	$0.15^{+0.06}_{-0.07}$	0.25	**NGC 5845**	$2.5^{+0.4}_{-0.5}$	$>^{+0.05}_{-0.05}$	0.23
NGC 3091	$6.2^{+5.2}_{-4.0}$	$>^{+0.02}_{-0.01}$	0.08	**NGC 5846**	$10.2^{+3.4}_{-3.7}$	$0.34^{+0.17}_{-0.18}$	0.20
NGC 3098	$3.9^{+1.3}_{-1.3}$	$0.14^{+0.08}_{-0.07}$	0.05	**NGC 5846A**	$12.3^{+4.7}_{-3.8}$	$0.17^{+0.22}_{-0.23}$	0.34
NGC 3115	$2.6^{+0.0}_{-0.6}$	$>^{+0.02}_{-0.06}$	0.09	NGC 5864	$5.0^{+1.0}_{-1.2}$	$-0.10^{+0.07}_{-0.06}$	-0.13
NGC 3156	$0.9^{+0.6}_{-0.3}$	$-0.17^{+0.14}_{-0.10}$	0.11	**NGC 5982**	$12.3^{+1.9}_{-2.0}$	$0.22^{+0.04}_{-0.06}$	0.19
NGC 3193	$5.7^{+1.7}_{-2.5}$	$0.48^{+0.04}_{-0.13}$	0.18	**NGC 6172**	$1.8^{+0.3}_{-1.0}$	$0.23^{+0.13}_{-0.07}$	0.01
NGC 3226	$>^{+3.4}_{-10.1}$	$-0.02^{+0.06}_{-0.07}$	0.31	**NGC 6411**	$8.3^{+0.4}_{-0.4}$	$0.15^{+0.05}_{-0.05}$	0.11
NGC 3245	$5.8^{+2.4}_{-2.7}$	$0.32^{+0.10}_{-0.09}$	0.29	NGC 7302	$4.0^{+1.0}_{-1.8}$	$0.33^{+0.10}_{-0.10}$	-0.04
NGC 3377	$3.6^{+0.4}_{-0.5}$	$0.35^{+0.05}_{-0.05}$	0.26	NGC 7332	$1.0^{+1.0}_{-0.8}$	$>^{+0.01}_{-0.29}$	-0.01
NGC 3379	$10.9^{+2.6}_{-2.8}$	$0.30^{+0.07}_{-0.08}$	0.21	**NGC 7454**	$2.8^{+1.3}_{-1.2}$	$0.13^{+0.08}_{-0.08}$	0.11
NGC 3384	$6.5^{+1.0}_{-1.6}$	$0.13^{+0.05}_{-0.04}$	0.21	NGC 7585	$1.3^{+0.8}_{-0.6}$	$>^{+0.14}_{-0.21}$	0.07
NGC 3412	$1.5^{+0.5}_{-0.5}$	$>^{+0.18}_{-0.10}$	-0.03	**NGC 7619**	$5.9^{+3.2}_{-2.0}$	$>^{+0.02}_{-0.13}$	0.13
				NGC 7626	$13.9^{+4.9}_{-2.4}$	$0.36^{+0.06}_{-0.05}$	0.29

Galaxy names in bold characters are ellipticals.
The > symbol represents a lower limit estimate: 15.0 Gyr in Age and 0.67 dex in [Z/H].
† Derived assuming model tracks of a constant age of 4 Gyr.

cantly – the resulting age/metallicity estimates. (Bressan *et al.* 1996; Trager *et al.* 2000a; T00b).

4.1 Errors

It is known that correlated observational errors can masquerade as real trends. Trager *et al.* (1998) have demonstrated the role of index errors in the determination of ages, metallicities and their correlations with velocity dispersion. Furthermore, the Balmer lines used to infer ages and metallicities in e.g. Hβ-[MgFe] diagrams, can be severely affected by emission and its correction is crucial to the determination of galaxy parameters. The general effect of correcting Hβ by the presence of emission is to change both the derived ages and metallicities. Age is reduced and [Z/H] increased ([α/Fe] is less affected). It happens so that the informa-

tion on Hβ errors is commonly used to separate and select the best galaxy data in the literature. The sample used by Trager *et al.* (1998) had a typical error of δHβ = 0.191 Å. A reasonable guide is that Hβ must be accurate to $\sim$ 0.1 Å to determine reliable ages and metallicities.

Our measured observational errors are not as small as González (1993, δHβ = 0.060 Å) or Kuntschner (1998, δHβ = 0.089 Å), although these are estimated errors. The average Hβ-index error in our sample is 0.11 Å. Our errors have been increased to account for uncertainties in the Hβ emission correction: previous to the emission correction our Hβ mean error was 0.086 Å.

It is important to emphasize here that in this work we focus our attention to conclusions drawn from the relative position of galaxies with respect to each other and not on absolute values.

The independent errors in the observables Hβ and [MgFe] from Figure 5 translate into correlated errors in the age *vs* metallicity plane. We have calculated the uncertainties in age and metallicity by interpolating new age and [Z/H] values for the points: (*Hβ−error*,[MgFe]), (*Hβ+error*, [MgFe]), (Hβ, *[MgFe]−error*) and (Hβ, *[MgFe]+error*). We show in Figure 8 that these four points describe well the uncertainties in the central age and [Z/H] determinations.

We have performed Monte-Carlo simulations of a large number of random points inside the 1σ error contour of a galaxy in the Hβ-[MgFe] plane. The random points were then interpolated using the TMB03 model grids; the age and [Z/H] values derived are plotted on the right-hand side panels of Figure 8. Note that the 1σ error ellipses on the Hβ-[MgFe] plane were transformed into rather twisted ellipses on the age-[Z/H] plane.

The age and [Z/H] values interpolated for (*Hβ−error*,[MgFe]), (*Hβ+error*, [MgFe]), (Hβ, *[MgFe]−error*) and (Hβ, *[MgFe]+error*) are also shown in the right-hand side panels. Although these four points do not describe perfectly well the total range of possible age and [Z/H] values inside the 1σ error ellipses, they do provide us with a sufficient sampling of the uncertainties involved when transposing errors from the Hβ-[MgFe] plane to ages or metallicities. We have then used the range of values from these four points as the uncertainty in age and [Z/H] determinations presented in Table 2.

We also show in Figure 9 how the error ellipses of Figure 8 are distributed in the total age-[Z/H] plane. Note that the slope of the error ellipses is very close to the direction of the spread of the points in the age and metallicity plane (we estimate Δ log *age* $\cong -1.57\ \Delta$ [Z/H]), indicating that correlated errors can masquerade as real trends.

5 THE [α/FE] RATIO

According to several authors, the central regions of giant E and S0 galaxies show an overabundance of α-elements over Fe, indicated in particular by the steep Mg_2 index radial gradients (Worthey, Faber & González 1992; Trager *et al.* 2000a; T00b). This finding strongly impacts on the theory of galaxy formation, as super-solar [α/Fe] ratios seem to require short star formation time-scales ($\lesssim$ 1 Gyr) that are hardly achieved by current models of hierarchical galaxy formation (e.g., Thomas & Kauffmann 1999).

The TMB03 predictions are identical to T00b Model 1, except that the latter do not include the α-element Ca in the α-element group. As pointed out by TMB03, the fractional contribution of Ca to the total metallicity is too small ($\sim$ 0.1 per cent) to change the isochrone and SSP characteristics.

Super-solar [α/Fe] ratios at fixed total metallicity are produced by a decrease of the Fe abundance rather than by an increase of the α element abundances ([Z/H] = [Fe/H] + A[α/Fe], where $A \equiv -\ \Delta$[Fe/H]/Δ[α/Fe]). The actual atomic abundance ratios of the so-called enhanced elements are in fact virtually solar; it is only the Fe-peak elements – which contribute $\sim$ 8% to the total amount of metals in the Sun – that are depressed (e.g., Trager *et al.* 2000a, TMB03). This result has been interpreted as being due to a fast early chemical enrichment, therefore dominated by Type II supernovae, in the nuclei of giant E and S0 galaxies. Alternative explanations, however, include a changing IMF slope and/or a changing binary fraction for Type I supernova production. Worthey (1998) discusses the possible scenarios thoroughly in his paper, and concludes that not all α-elements follow the Mg trend. Worthey (1998) even suggests the existence of a third chemical enrichment source (perhaps another type of SN) other than SN Type I and II, to explain the behaviour of N or of the V, Sc, Ti trio in the $TiO_{1,2}$ bands. Comparing [Mg/Fe] ratios from spiral bulges (McWilliam & Rich 1994; Jablonka *et al.* 1996), S0s and elliptical galaxies in the literature (Davies *et al.* 1993; Carollo & Danziger 1994; Fisher *et al.* 1995, 1996), the data available to date seem to indicate that [Mg/Fe] is near zero in most galaxies of all types with velocity dispersion less than $\sim$ 200 km/s (Worthey 1998).

We will examine below the behaviour of some important indices with varying [α/Fe] models. In Figure 10 the indices of the α-element group are plotted against the average iron index <Fe>. These diagrams are almost degenerate in age and metallicity, and so are ideal to identify [α/Fe] variations by comparing TMB03 models with [α/Fe] = 0.0 and +0.3.

Assuming that the difference in central velocity dispersion σ_0 is determined by the depth of the gravitational potential and ultimately the mass of the galaxy, we separate galaxies according to mass in Figure 10 by assigning different symbols for galaxies with σ_0 smaller (filled circles) or greater (open circles) than 225 km/s.

The formal [α/Fe] ratios per galaxy were determined by interpolating [α/Fe] values from the almost degenerate model grids in the Mg_2/<Fe> and Mg b/<Fe> diagrams, and averaging the resulting values. The interpolation is performed between TMB03 models with [α/Fe] = 0.0, +0.3, +0.5 and assuming, for simplicity, only model tracks for an average age of 4 Gyr (i.e., to make the interpolation easier; other model tracks do not alter the results because the Mg/Fe plane is strongly degenerate). We present the derived [α/Fe] for the galaxies in our sample in Table 2. It is very difficult to estimate errors for this determination of [α/Fe], but examining the errors in Mg and Fe-indices, we assume that on average $\pm$ 0.05 dex in [α/Fe] is a very safe upper limit estimate of the uncertainty.

We find that the maximum magnitude of the [Mg/Fe] overabundance is around 0.3 dex, for the central $r_e/8$ extraction. In general, even galaxies with $\sigma_0 < 225$ km/s show Mg enhancement with respect to Fe, and the distinction of both samples (with $\sigma_0 < 225$ km/s and with $\sigma_0 > 225$ km/s) is not always clear in Figure 10. The NaD and CN indices, trac-

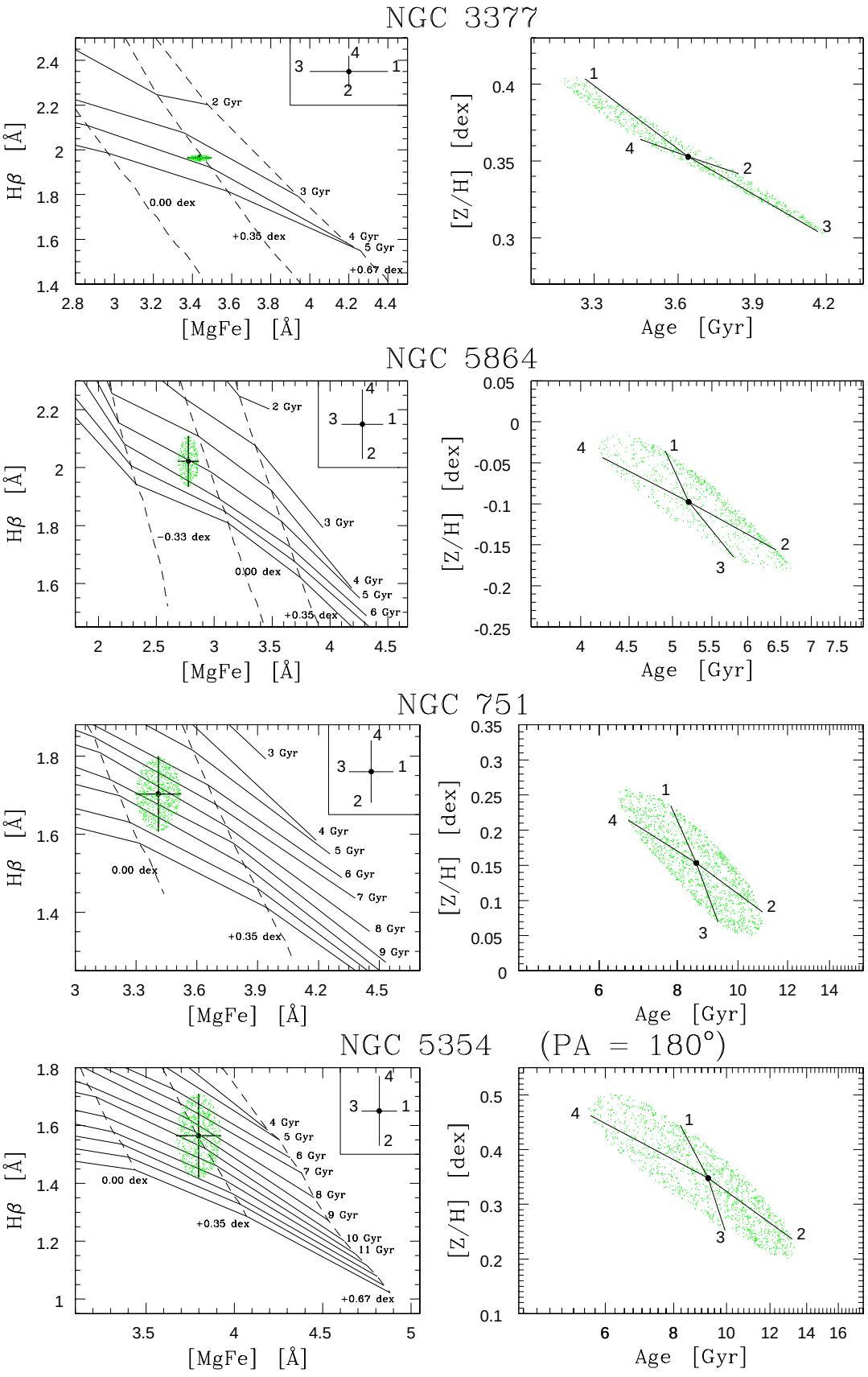

Figure 8. Examples of index errors transposed to the age-metallicity diagram. The [MgFe]-Hβ plane is shown on the left-hand side and overplotted are the model grids of TMB03. In each plot we show the position of a galaxy and its error bars in the index-index plane. On the right-hand side panels we show the results of the model grid interpolation to the age-metallicity plane. The 1σ error ellipses were obtained from Monte Carlo simulations.

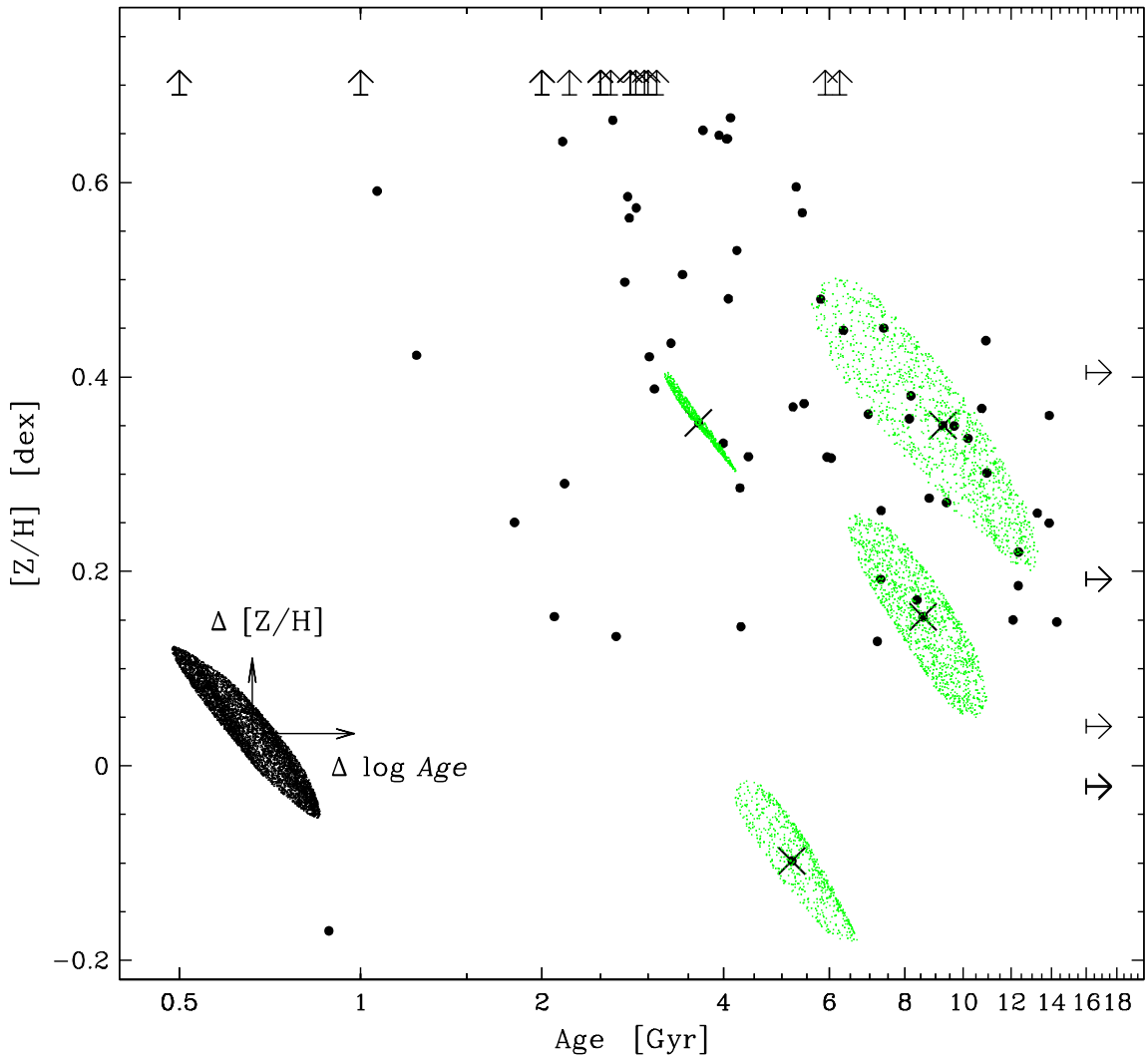

Figure 9. Age-metallicity diagram with error ellipses. The error ellipses are the same shown for four galaxies in Figure 8. The slope of the error ellipses is nearly the same as the slope of the overall tendency between age and metallicity (we estimate Δ log *age* $\simeq -1.57\ \Delta$ [Z/H]), showing that correlated errors can masquerade as real trends.

ers of Na and mainly N respectively (Tripicco & Bell 1995, Worthey 1998, TMB03), show the same type of behaviour as Mg with respect to Fe. It appears that Na is more enhanced than Mg, or simply that our measurements are suffering from NaD absorption by interstellar material. Except for a few of the less massive galaxies ($\sigma_0 < 225$ km/s) the rest show α-element enhancement (see Figures 10 and 11). The Ca4227 and Ca4455 indices barely overlay the models for [α/Fe] = 0.0, and their different behaviour with respect to the other indices cannot be assigned to [α/Fe] enhancement. Both indices are not well calibrated for galaxies, and not convincingly either for globular clusters (Maraston *et al.* 2003). Ca4227 is sensitive mainly to N, and its Ca-element dependence is yet to be shown. As for Ca4455 – which is *insensitive* to Ca abundance (Tripicco & Bell 1995), Fe and Cr seem to be the main contributors. The TiO model indices are almost degenerate in the [α/Fe] sensitivity, and are badly calibrated even for globular clusters in Puzia *et al.* (2002).

In summary, if large [α/Fe] ratios require short star formation time scales for the galaxies, we can say from Figure 10 that, in our sample of mostly low-density environment galaxies, massive early-type galaxies (high σ_0) do not obviously have more rapid star formation (high [α/Fe]) than small (i.e., less massive) early-types, as predicted by hierarchical galaxy formation models.

Figure 11 shows the relations of the [α/Fe] ratio with age, metallicity, velocity dispersion and magnitude per galaxy. There is a trend in that older galaxies are strongly overabundant whereas younger galaxies approach solar abundance ratios (Figure 11-a). A Spearman rank correlation test results in $\rho = 0.38$ with more than 90% probability that a correlation is present. It is necessary to note, nevertheless, that part of this correlation may be due to the correlated errors discussed before.

The median [α/Fe] ratio for the 50 Es is 0.19 ± 0.08 dex, and for the 30 S0s it is 0.11 ± 0.11 dex, the uncertainties are the rms values.

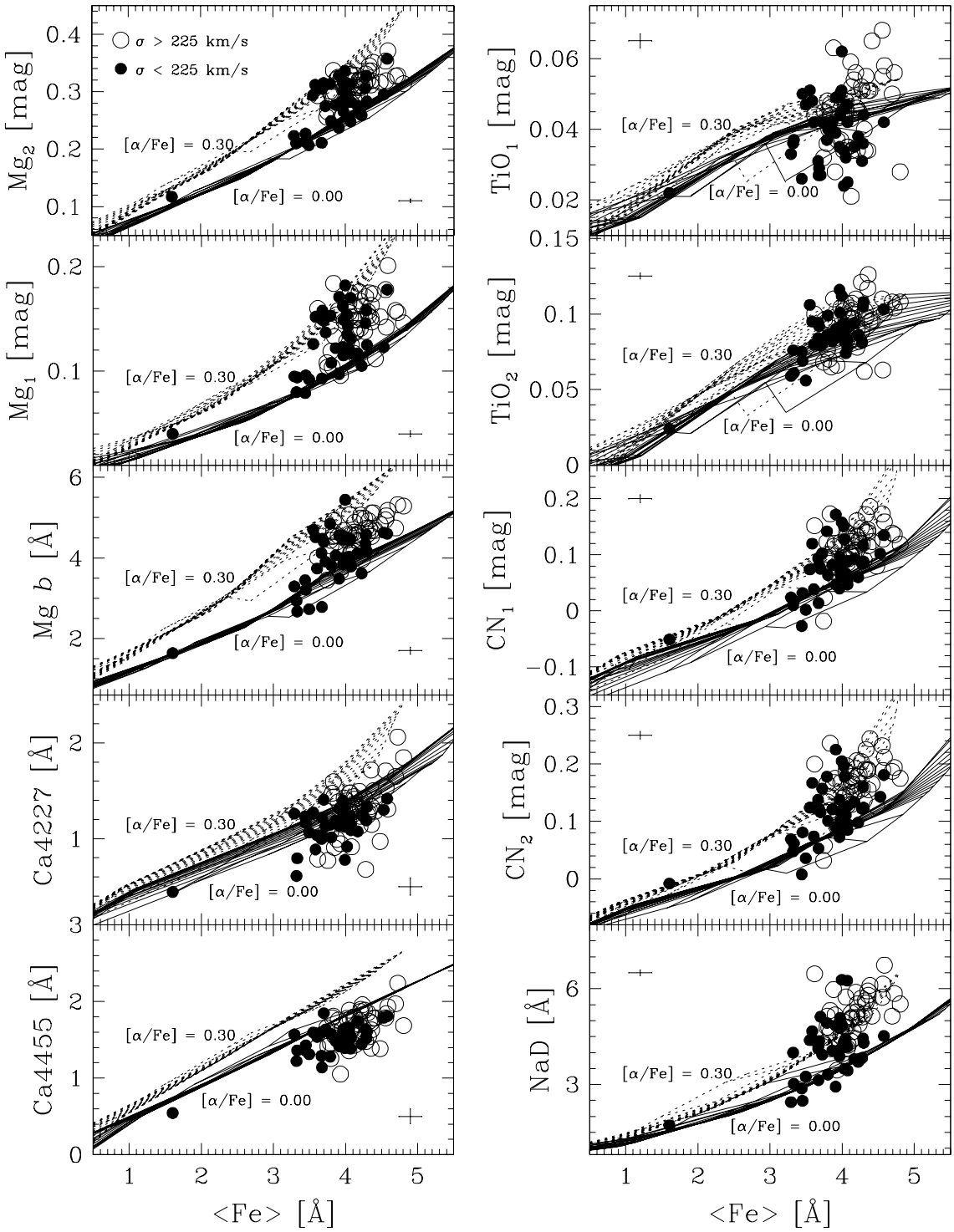

Figure 10. Index tracers of α-elements *vs* <Fe>. Overplotted are the α-enhanced SSPs by TMB03 for [α/Fe]=0.0 (solid lines) and [α/Fe]=+0.3 (dashed lines). The symbols separate galaxies with σ_0 smaller or greater than 225 km/s, as indicated in the top-left panel. The outlier galaxy on the bottom-left of all panels is NGC 3156.

Trager *et al.* (2000b, T00b), analysing the sample of mainly "field" elliptical galaxies from González (1993), claimed that [α/Fe] depends only on σ_0 and not on age. However, Figure 11-a suggests a SNe II/SNe Ia enhancement ratio higher in the older galaxies of our sample; in other words, there is a hint that older galaxies had short star-formation time scales. On the other hand, there is no clear correlation of [α/Fe] with metallicity in Figure 11-b.

T00b found that [α/Fe] and σ_0 are highly correlated (linear) quantities. Their proposed linear fit to the relation

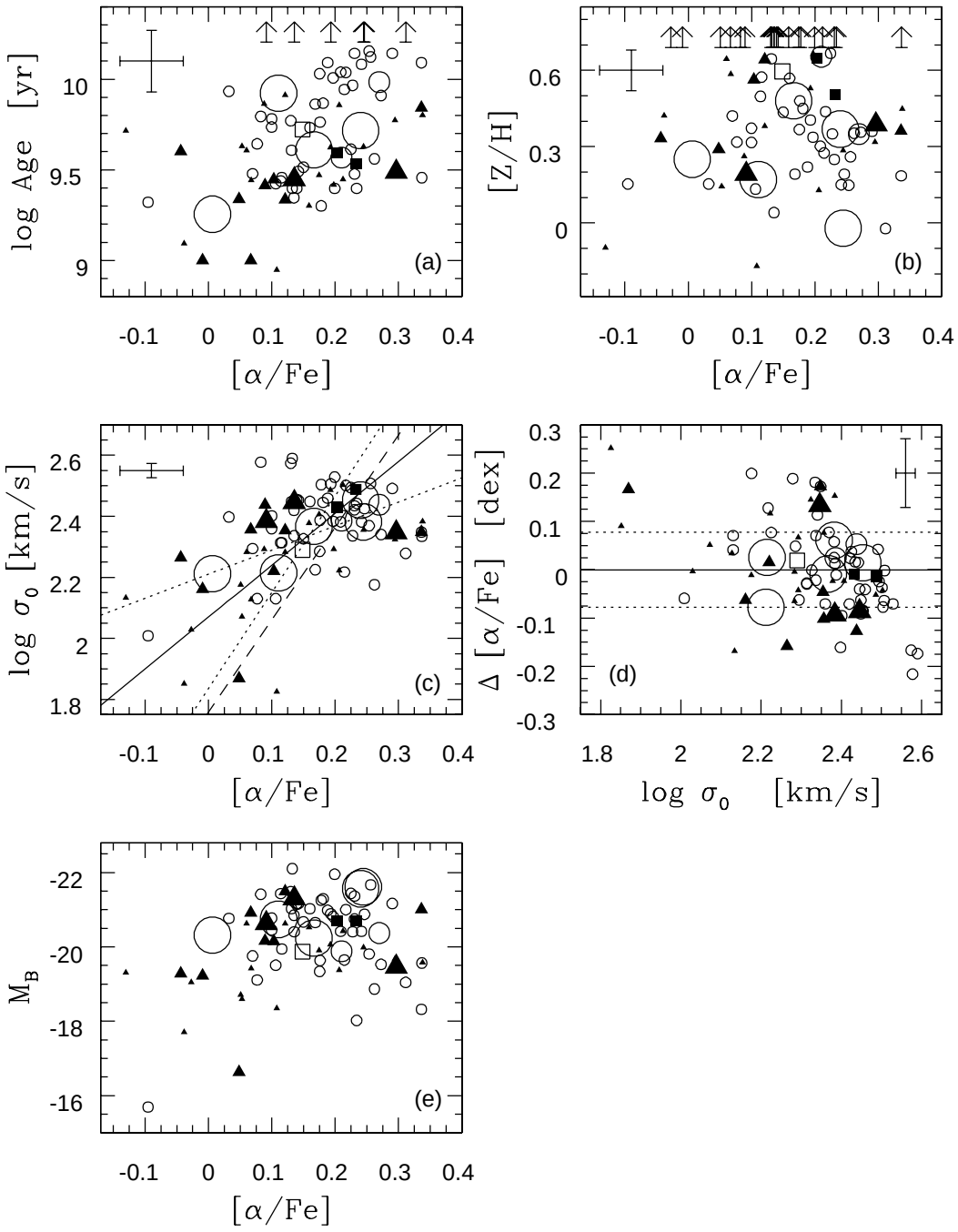

Figure 11. Correlations of the enhanced element ratio [α/Fe] with (a) age, (b) metallicity, (c) velocity dispersion and (e) absolute magnitude. Panel (d) shows the scatter about the solid line fit from panel (c) and the dotted lines represent the 1σ scatter (Δ[α/Fe]=0.079 dex. The median [α/Fe] ratio of the sample is 0.17 dex. Circles represent elliptical galaxies and triangles are S0-type galaxies in the sample. Large circles and triangles are isolated galaxies, medium size denote field, and the smallest symbols represent group galaxies. The three Virgo cluster galaxies in the sample, NGC 4365, NGC 4374, NGC 4754, are plotted as square symbols (open square denotes S0, filled square denotes E). The error bars represent the mean uncertainties in log Age (0.17 dex), [Z/H] (0.078 dex), log σ_0 (0.024 dex) and [α/Fe], for which we assume the error estimate of 0.05 dex.

is shown by the dashed line in Figure 11-c. Examining panel (c) one cannot safely conclude that the previously discussed trend in [α/Fe] is as prominent: we find the linear correlation coefficient R = 0.63. Most of the spread in Figure 11-d seems consistent with the errors, thus, for a given σ_0 most (but not all) galaxies have a similar [α/Fe] within the errors. The existence of [α/Fe] ratio variations at a given central velocity dispersion would imply that the star-formation history of old galaxies at a given σ_0 is not entirely homogeneous. The [α/Fe]-σ_0 fit to our sample is shown by the solid line in Figure 11-c (slope: 1.7). We have used the bisector (solid line) of the regressions of [α/Fe] on σ_0 and σ_0 on [α/Fe]

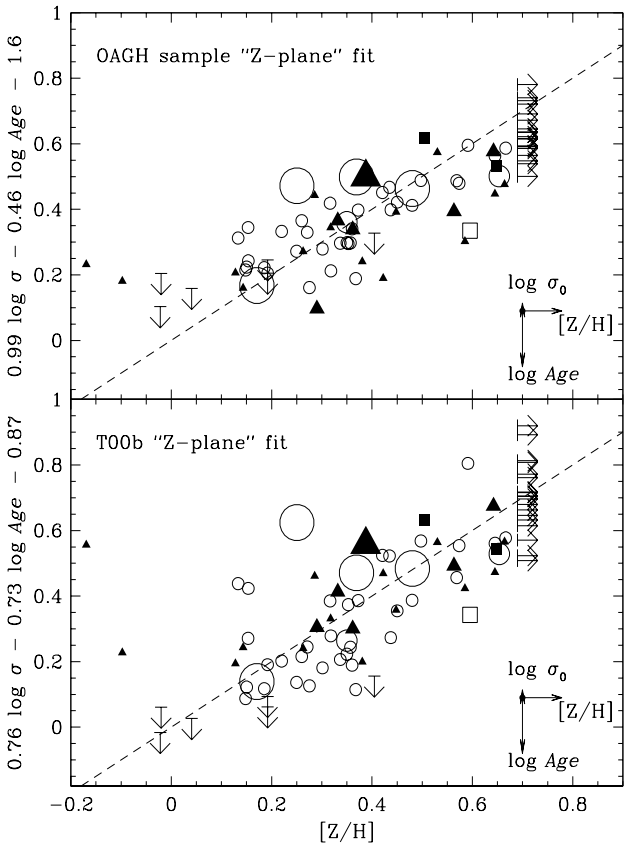

Figure 12. The edge-on view of the metallicity-age-σ plane. The dashed line in the top panel is the fit to our data points and defines the plane as [Z/H] = 0.99 log σ_0 – 0.46 log *Age* – 1.60. The dashed line in the bottom one is the fit in Trager *et al.* (2000b). Vectors of 0.17 in log Age, 0.078 dex in [Z/H] and 0.024 in log σ_0 represent the average of the overall uncertainties in our sample. The symbols are the same as in Figure 11.

(represented by the two dotted lines in panel *c*). Panel (d) shows the residuals of the [α/Fe]-σ_0 relation (with respect to the solid line of panel *c*); the 1σ scatter of the relation is Δ [α/Fe] = 0.079 dex, and is represented by the dotted lines in panel (d).

In Figure 11-e we present the weak relation between [α/Fe] and absolute blue magnitude. There is quite a large range of magnitudes for oversolar [α/Fe] values.

In sum these results reinforce the picture of very old and massive galaxies having formed in relatively short time scales with small scatter in their [α/Fe] values.

6 [Z/H], AGE, σ_0 AND [α/FE] HYPERPLANE

In a very interesting paper, Bressan *et al.* (1996) explored the four dimensional space which involved Hβ, [MgFe], (1550-V) and log σ_0 in elliptical galaxies. Forbes & Ponman (1999) were among the first to explore the relation between σ_0 and stellar population age derived from model comparison. Later, T00b performed a principal component analysis (PCA; other references to PCA: Whitney 1983, Ronen *et al.* 1999) on four variables, namely log σ_0, log *Age*, [Fe/H] and [E/Fe]; i.e. velocity dispersion, age, metallicity and element-enhanced ratio which they called E/Fe (here we adopt the notation α/Fe). T00b found that most of the variance (91 percent) in their sample of local ellipticals can be explained with just two parameters, i.e., the sample is basically bi-parametric in the four-dimensional space σ_0, *Age*, [Fe/H] and [E/Fe], in other words, the galaxies are located in a hyperplane in this four-dimensional space that they named, the metallicity hyperplane.

Table 3. Principal component analysis: the hyperplane.

	log σ_0	log Age	[Z/H]	[α/Fe]
Covariance matrix:				
log σ_0	1.0000	0.5944	0.4290	0.5757
log Age	0.5944	1.0000	-0.1919	0.5097
$[Z/H]$	0.4290	-0.1919	1.0000	0.1709
$[\alpha/Fe]$	0.5757	0.5097	0.1709	1.0000
PCA results:				
	PC1	PC2	PC3	PC4
log σ_0	0.6135	0.1700	0.3938	0.6630
log Age	0.5154	-0.4987	0.3875	-0.5792
$[Z/H]$	0.2206	0.8477	0.0887	-0.4742
$[\alpha/Fe]$	0.5561	-0.0616	-0.8288	-0.0065
Eigenvalue	2.139	1.1668	0.4621	0.1654
Variance	0.5438	0.2966	0.1175	0.0421
Cumulative	0.5438	0.8405	0.9579	1.0000

Given the importance of this finding, we have performed a PCA in our sample data. The results are presented in Table 3 and Figure 12.

It is interesting to note from an inspection of the covariance matrix that while log σ is significantly correlated to the other three variables (log Age, [Z/H] and [α/Fe]), both log Age and [α/Fe] are not correlated to [Z/H] in our sample. A similar conclusion regarding the behaviour of log σ_0, [Z/H] and log Age can be obtained from Figure 13 where the panels show the sample segregated according to σ_0.

The least square fit to our hyperplane is:

$$[Z/H] = 0.99(\pm0.15) log\sigma_0 - 0.46(\pm0.08) log Age - 1.60(\pm0.40) \quad (1)$$

In linear terms, this equation can be translated to the approximate law:

$$Z \propto \sigma_0 \cdot Age^{-0.5} \quad (2)$$

If we assume constant values for σ_0 and plot eq. 1 in the Age-metallicity plane, we find the interesting relations shown in Figure 13. The existence of the Z-plane indicates that there exists an age–metallicity relation *for each value of* σ_0. This relation implies, as shown in Figure 13, that at a fixed σ_0, metal-rich galaxies have a younger stellar population in their central regions. T00b have found the projection of the hyperplane to be [Z/H] = 0.76(±0.13) logσ_0 - 0.73(±0.06) log *Age* - 0.87(±0.30), where *Age* is always taken in Gyr.

From the correlation matrix, the strongest effect seems to be a change in log age (and not in [Z/H]) in the sense that age increases going from small σ_0 ellipticals to large σ_0 ones. Even though there are several lower limits in the right panel of Figure 13 (massive galaxies that fall outside

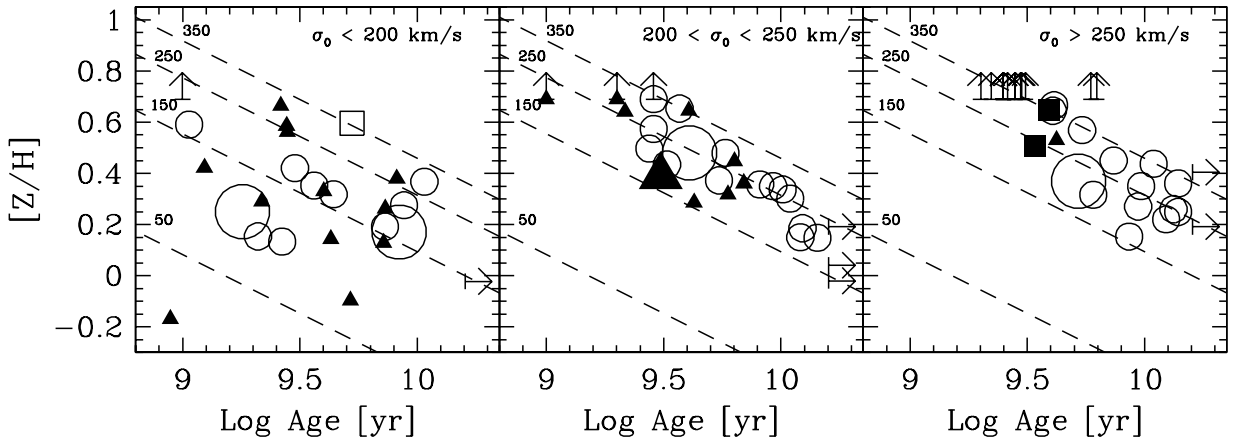

Figure 13. Age-metallicity plane for constant σ_0. Circles represent elliptical galaxies and triangles are S0-type galaxies in the sample. Large circles and triangles are isolated galaxies, medium size denote field, and the smallest symbols represent group galaxies. The three Virgo cluster galaxies in the sample, NGC 4365, NGC 4374, NGC 4754, are plotted as square symbols. The panels separate the galaxies in bins of σ_0; the dashed lines are fits from eq. 1, assuming constant σ_0 values as labelled.

the model grids) the effect is visible between the left and central panels.

This is an interesting result, and cannot be a reflection of the well known Mg-σ relation. If that was the case one would expect a stronger correlation between σ_0 and metallicity, given that Mg is the dominant index in the [Z/H] estimate in this work using TMB03 models.

Nevertheless, one must be aware in dealing with projections of hyperspaces that the apparent correlation may only be the product of the distribution of points in the hyperspace projected onto a particular plane.

To answer this point we performed a Principal Components Analysis, the results of which are given in Table 3. The first two principal components contain 84 percent of the total variance indicating that the ellipticals in our sample are distributed in a flattened volume in the 4-D space. This is further illustrated in Figure 14 where we show the face-on and edge-on views of the projected variables. To simplify comparisons with T00b we have used similar orientation in our diagrams. It is interesting how similar are our results and those of T00b, strengthening the reality of the metallicity hyperplane.

Summarising, metallicity is a linear function of both log *Age* and log σ_0, i.e., $Z \propto \sigma_0 \cdot Age^{-0.5}$, which defines the so called "Z-plane". Following the fit we derived for our sample, the contours of constant σ_0 have the slope $\Delta \log Age \approx -2.2 \Delta$[Z/H]. This is close to the "3/2 relation" of Worthey (1994), which expresses trajectories in the log *Age* - [Z/H] space along which colours and line-strengths remain roughly constant. Thus, the Z-plane correlation predicts that line-strengths should be constant along trajectories of constant σ_0 in the Z-plane.

The enhancement ratio, [α/Fe], is a linear function of log σ_0, increasing towards high-σ_0 galaxies, and should be also responsible for some of the scatter in Figure 12.

7 DISCUSSION

Kuntschner (1998) found that the Fornax cluster elliptical galaxies appear to be roughly coeval with some evidence for slightly younger ages for the most metal-rich ones. Using Lick/IDS indices and Worthey (1994) SSP models, he estimated the ages to be around 8 Gyr, and the galaxies showed a sequence of metallicities from -0.1 to +0.35 in [Fe/H]. This result is consistent with the conventional view of old, coeval elliptical galaxies where the metallicity scales roughly with the size of the galaxy. However, the lenticular galaxies in Fornax have *luminosity weighted* ages that are smaller than those of the ellipticals, spanning from less than $\sim$ 2 Gyr to 8 Gyr, and also covering a large range of metallicities from -0.5 < [Fe/H] < +0.5. For the purpose of comparison with literature data, Kuntschner (1998) also observed the galaxy NGC 3379. The age of NGC 3379 in Kuntschner's analysis is $\sim$ 8.4 Gyr, whereas we have estimated $\sim$ 10.0 Gyr (with TMB03 models). We feel that comparing age estimates from different authors (which may have used different models) is not a reliable procedure; to check for systematic differences between cluster and field environment we prefer to compare the distribution of the galaxies in the [MgFe]-Hβ plane with the Fornax sample distribution, as both are in the Lick/IDS index system.

In Figure 15 we show a comparison between Hβ and [MgFe] indices for the Fornax and OAGH samples. The bottom panel of Figure 15 shows only S0 galaxies in both samples, and the right-hand panel shows only elliptical galaxies.

We estimate that the average age for our sample of group, field and isolated galaxies (5.8 Gyr) is younger than Fornax cluster ellipticals ($\sim$ 9-10 Gyr). Secondly, both Es and S0s in our sample cover a large range of ages *and* metallicities. Although our galaxies span wider ranges in age and [Z/H] than the Fornax galaxies, the Es and S0s in the OAGH sample appear to have on average more similar stellar populations than the very distinct behaviour of Es and S0s in Fornax.

In Section 4 we have estimated that S0s present a younger *mean* age than Es. It is important to emphasize here that the line-strength indices reflect only the integrated,

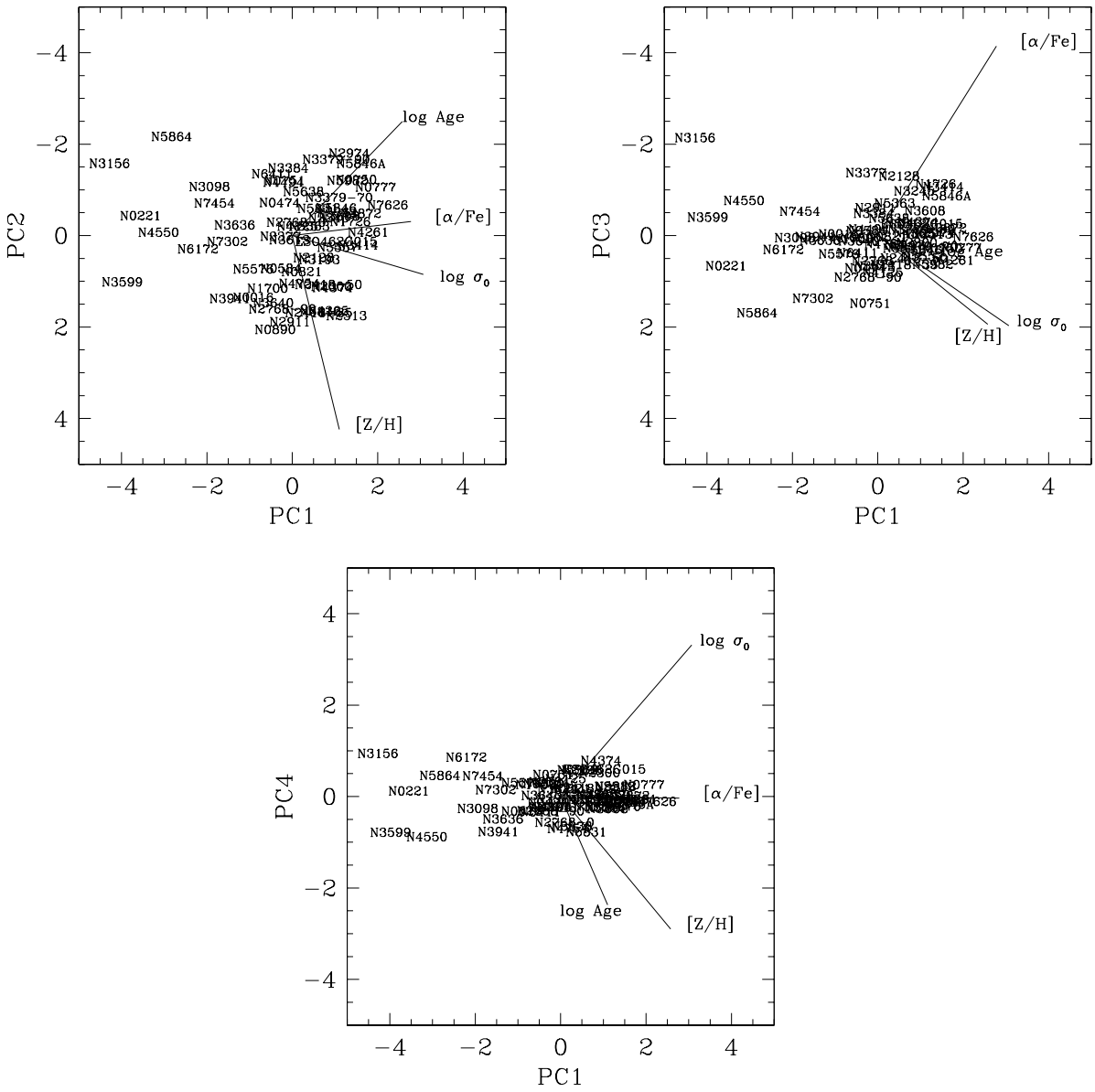

Figure 14. Principal Component Analysis results on the OAGH sample. The position of the galaxies in the diagrams is denoted by their names. The top panels represent the face-on (right) and edge-on (left) projections of the log *Age*-[Z/H]-log σ-[α/Fe] hyperplane. Projections of the four basic variables are shown as arrows in the direction of increase (for log *Age*, this arrow points in the direction of older galaxies). Velocity dispersion and enhancement ratio dominate the first principal component (PC1), while age and metallicity dominate the second (PC2). The third (PC3) and fourth (PC4) principal components contribute less than 12% to the overall variance in the log*Age*-[Z/H]-log σ-[α/Fe] space.

luminosity weighted properties in a galaxy. As young populations are more luminous per unit mass than old ones, a *small* (in mass) young population can dramatically change the strength of indices, in particular Hβ. de Jong & Davies (1997) and Trager (1997) have demonstrated this and also showed that the strong Hβ galaxies in González (1993) sample tend to have disky isophotes. de Jong & Davies (1997) suggested that ongoing star-formation might be associated with the presence of a disk. In the OAGH sample, elliptical galaxies that present young ages and hints of a stellar disk are NGC 315 (Peletier *et al.* 1990; our age: 2.5 Gyr), NGC 584 (Michard & Marchal 1994; 3.8 Gyr), NGC 720 (Goudfrooij *et al.* 1994; 3.0 Gyr) , NGC 821 (Ravindranath *et al.* 2001; 4.0 Gyr), NGC 3377 (Scorza 1993; 3.6 Gyr), NGC 3610 (Scorza & Bender 1990; 1.8 Gyr), NGC 3613 (Goudfrooij *et al.* 1994; 5.6 Gyr), NGC 3640 (Goudfrooij *et al.* 1994; 2.5 Gyr), NGC 4365 (Forbes *et al.* 1995; 3.6 Gyr), NGC 4374 (Zirbel & Baum 1998; 3.8 Gyr), NGC 5322 (Goudfrooij *et al.* 1994; 2.4 Gyr), NGC 5845 (Reid *et al.* 1994; 2.5 Gyr), i.e., 60% of elliptical galaxies with ages younger than 4 Gyr show photometric evidence of a stellar disk component in their morphologies.

NGC 3156 has a very distinct behaviour with respect to the bulk of the sample. As we have noted in some plots, this is the youngest and most metal-poor elliptical galaxy in the sample (NGC 5864 shows equivalently low metallicity

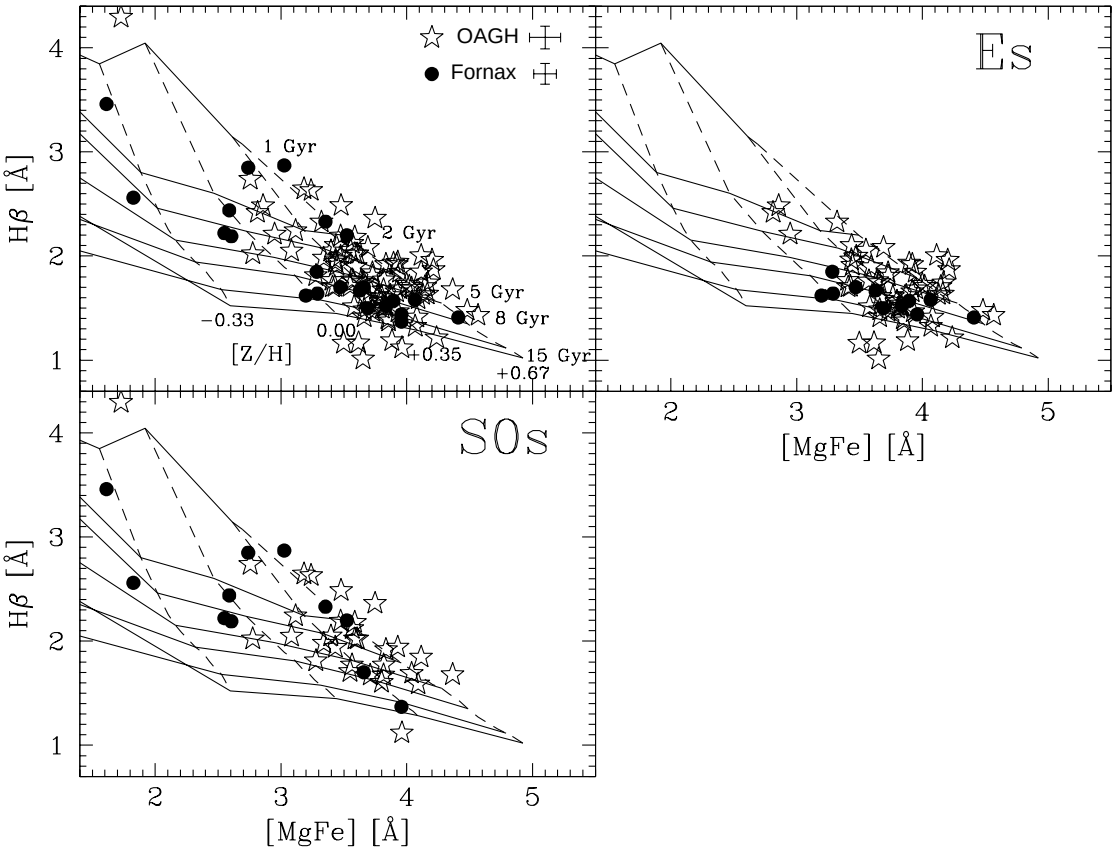

Figure 15. Comparison between the distribution in the Hβ-[MgFe] plane of Fornax and OAGH samples. The model grids are from TMB03, with [α/Fe] = 0.0, in age steps of 1, 2, 3, 5, 8, 12, 15 Gyr and metallicity steps of -0.33, 0.00, +0.35 and +0.67 dex. The bottom panel shows only S0 galaxies in both samples, and the right-hand panel shows only elliptical galaxies.

but with larger error bars, and substantially older age). According to the calculations of Poggianti & Barbaro (1997) *strong* Balmer absorption is created mainly at the main sequence turn off and cannot originate from other evolutionary stages (at least not for relatively young systems). Note that we are referring to *strong* Balmer absorption in a galaxy with a *young* stellar population. In many cases, Horizontal Branch (HB) stars can affect Balmer lines rather severely (see Maraston *et al.* 2003 for TMB03 model calibration of the Balmer lines). However, in the case of NGC 3156 it would be necessary to have a significant population of HB stars to produce such a young age. In fact, Maraston *et al.* (2003) have determined rather old ages ($\sim$ 8 Gyr) for two globular clusters NGC 6441 and NGC 6388 which are known to exhibit an important tail of warm HB stars. Furthermore, Burstein *et al.* (1988) have shown that the ultraviolet excess in early-type galaxies (which is now known to be associated with HB stars; O'Connell *et al.* 1999) correlates well with Mg_2 (NGC 3156 shows weak Mg_2 absorption [cf. Paper I], and poor metallicity). Hence we believe that the young age estimated from the model predictions for NGC 3156 is reliable. This is a disk dominated S0 galaxy, with a dusty and faint bulge, located in a group and shows no obvious interaction features. It is a galaxy that shows a high V/σ_0 value (=1.2; Paper I).

The relations between Age and metallicity [Z/H] against velocity dispersion and absolute blue magnitude (calculated from apparent magnitudes and our determinations of radial velocity given in Paper I, and assuming H_o = 75 km/s/Mpc) are shown in Figure 16. We observe a trend in that the oldest and more metal rich galaxies tend to have higher velocity dispersions. Caldwell, Rose & Concannon (2003) and Trager *et al.* (2000a,b) claim that there is a trend for lower σ_0 (or less massive elliptical) galaxies to have younger ages, contrary to what is found by Kuntschner (2000) and TF02 with their samples. Caldwell *et al.* (2003) also note a modest (if any) trend in [Z/H] with σ. Ours and these previous results, however, are not conclusive enough to place key constraints on age distributions predicted by numerical simulations of galaxy formation, but we refer the reader to a discussion of this point in TF02.

In Section 5 we have seen that there is a marginal tendency for massive galaxies to show larger [α/Fe] values than less massive ones. Worthey (1992,1998) detail several processes that can produce an α-element enhancement as a function of galaxy mass. They are mostly related to the different contributions towards the chemical enrichment of galaxies by supernovae types Ia and II. SN Ia (with progenitors less massive than 5-10 $M_\odot$) release Fe-peak elements after a time delay of about a few times 10^8 years. Type II supernovae, on the other hand, originate from more massive stars and contribute earlier to the abundance of α-elements

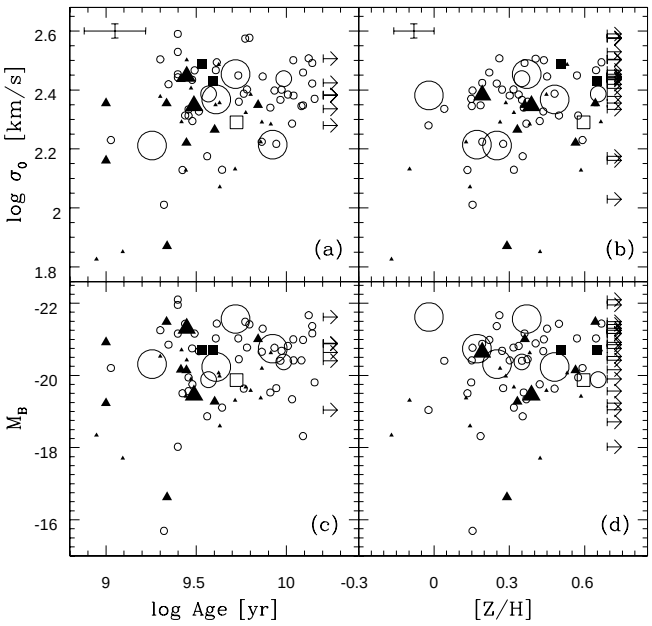

Figure 16. Panels *a* and *b* present the central velocity dispersion against Age and metallicity determinations for the $r_e/8$ aperture extraction. Panels *c* and *d* show the absolute blue magnitude against Age and [Z/H]. The symbols are the same as in Fig.11.

and Fe. The ratio of SNe type II to type Ia, which can vary from massive to less massive galaxies, somehow determines the [α/Fe] abundances. There are several scenarios proposed for the variation of type II/type Ia ratio (e.g. Arimoto & Yoshii 1987) including winds, amount of binaries, even IMF variations due to environmental causes. Different time-scales for the formation of SNe Types II and Ia, allow the prediction of a correlation of Mg strength with dynamical crossing time (Worthey 1998) or, if including the effects of winds (Arimoto & Yoshii 1987) with the potential well of the galaxy. An environmentally controlled IMF predicts good correlation with σ (Paper I). While Mg_2 versus σ is a well known tight correlation, <Fe> versus σ is weaker. This suggests that the basic relation is between the Mg abundance and the velocity dispersion. Contrary to Worthey (1998), who finds that [Mg/Fe] vs. σ does not depend on galaxy type, supporting the statement above, we find that ellipticals have [α/Fe] ratios slightly higher than S0s, on average.

Other indices that correlate well with σ are NaD and CN (Worthey 1998). Matteucci & Padovani (1993) claim that a change in the IMF slope of 0.4 could produce a 0.3 dex change in α-element abundances. It remains to be proved that such a change in the IMF slope could be consistent with observations.

The metallicity of the interstellar medium can provide a constraint to decide between the time formation difference hypothesis and the IMF variation one (Worthey 1998). We have to resort to X-ray abundance determinations where we encounter difficulties with modelling the Fe atom (Loewenstein & Mushotzky 1996; Arimoto *et al.* 1997) although progress has been achieved in that direction (Matsushita *et al.* 2000).

Finally, in the previous Sections we have seen that, in general, high and low density environment galaxies (the former in groups and the latter field or isolated) have similar distribution in the Age-[Z/H], Hβ-[MgFe], Hγ-[MgFe] planes, thus suggesting that dynamical interactions are not a necessary driver for the observed variations. If this is true, it confirms Longhetti *et al.* (1998a,b, 1999, 2000) who reached the same conclusion by examining the line-strength indices of 51 early-type galaxies (21 shell galaxies and 30 members of pairs displaying clear signatures of interaction) and comparing them with the reference sample of "normal" galaxies by González (1993).

One should be prudent not to overinterpret these results, as the truly isolated galaxy statistics in our sample is limited by small number effects. We could in fact claim to be seeing a different distribution on the Hβ,[MgFe] plane for Fornax as compared with our isolated/field/group galaxies in Figure 15.

Our new data seem to be showing a trend for massive (isolated/field/group) galaxies to be older (Figure 13 and 16-a) and display greater α/Fe values (Figure 11-c).

8 A BROAD PICTURE OF GALACTIC CHEMICAL EVOLUTION

Understanding the broad picture of galactic chemical evolution will require us to firm up the links between the chemical abundances of predominantly active star-forming systems (i.e. spirals) and predominantly quiescent ones (i.e. ellipticals, spheroids, lenticulars and bulges).

While a common elemental yardstick may not exist because of the different elements which we observe directly in each galaxy type, it may be possible to tie the two types together abundances-wise by observing elements in each which share the same nucleosynthesis production site. An example might be oxygen and magnesium. In external spirals oxygen is taken as the metallicity gauge primarily because of its observability. Magnesium, which, like oxygen, is primarily produced in massive stars (Nomoto *et al.* 1997a,b) may be measurable directly through a calibrated Mg_2 index. Then oxygen and magnesium might be linked by assuming a "cosmic" Mg/O ratio calibrated locally. Some features in the optical spectra of elliptical galaxies that contain oxygen signatures are G4300 and $C_2$4668, in the near-infrared there is also the 2.3 μm CO feature. As synthetic spectra and stellar abundances grow more precise, the contribution of specific elements to the indices might be measurable, leading to a much more clear understanding of chemical enrichment and galaxy formation.

In what follows we have used the Hα line information in our spectra of early-type galaxies to estimate the oxygen abundance using the N2 ratio as in Denicoló, Terlevich & Terlevich (2002). We have derived the metallicity [Z/H] for our ellipticals and S0s in Section 4 (this metallicity comes mainly from Mg and Fe abundances), so it is an interesting exercise to compare both [Z/H] metallicity and O abundance estimate for early-type galaxies.

The N2 calibrator is defined as the logarithmic ratio of the emission lines [N II] λ6584 to Hα. In the elliptical galaxies, we have measured [N II] and Hα as indices. The N2 is the logarithmic ratio of fluxes and not equivalent widths, so we have computed fluxes from the index definitions as stated in eq. 11 of Paper I. We have only used [N II] and Hα in-

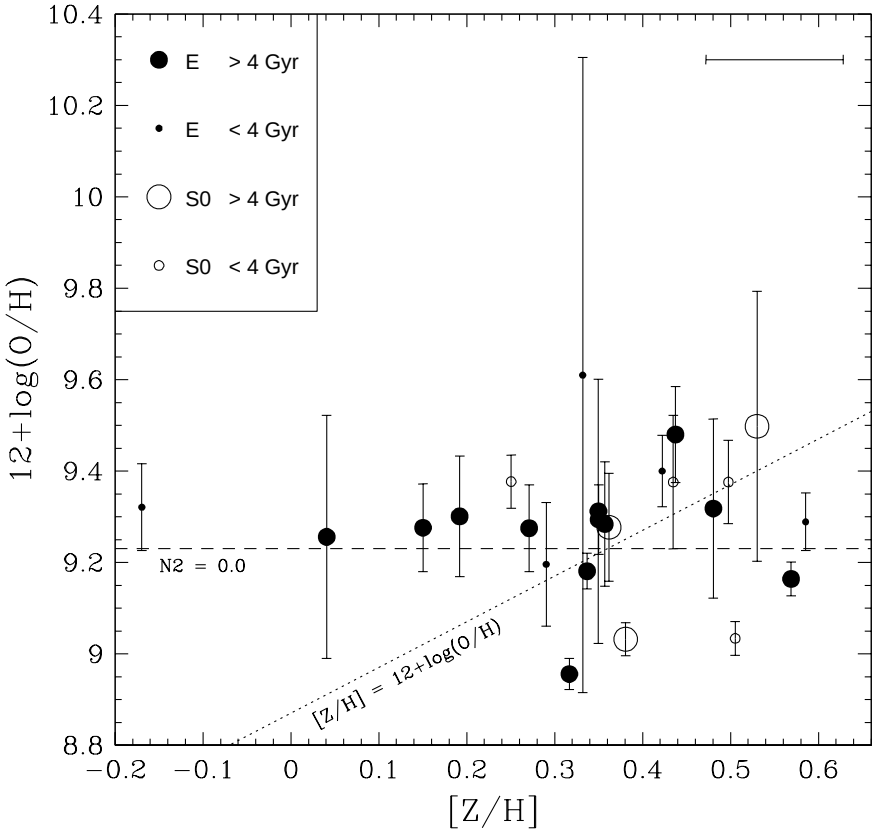

Figure 17. Oxygen abundance *vs* metallicity [Z/H]. The oxygen abundance was derived from the [N II] and Hα index measurements in the spectra of our early-type galaxies using the N2 calibrator. The [Z/H] metallicity is the result of the interpolation of Thomas *et al.* (2003) SSP models for measurements in galaxy spectra within the $r_e/8$ aperture. Solid circles indicate elliptical galaxies, open circles are S0s. The size of the points is associated with the galaxy age (ages are from Table 2). The dotted line indicates when 12+log(O/H) is equal to [Z/H]. The dashed line represents 12+log(O/H) when N2 is null.

dices with negative values (i.e. lines in emission). The errors in the [N II] and Hα indices are derived from repeated measurements. The 12+log(O/H) abundances were derived from 12+log(O/H) = 9.23($\pm$0.02) + 0.79($\pm$0.03)$\times$N2 (Denicoló, Terlevich & Terlevich 2002). In Table 4 we show the oxygen abundance and [Z/H] metallicity, for the galaxies with [N II] and Hα indices in emission.

In Figure 17 we present the 12+log(O/H) *vs* [Z/H] diagram. The plot supports substantial oversolar abundances for the interstellar medium (ISM) as measured from 12+log(O/H). If we take the Solar value of $12+\log(O/H)_\odot$ = 8.87 (Grevesse *et al.* 1996), and by definition $[Z/H]_\odot = 0.0$, we draw the dotted line in Figure 17 where 12+log(O/H) = [Z/H]. The distribution of points indicates that most galaxies have Z(ISM) > Z(stars), where we use here "Z" to loosely describe metallicity; Z(stars) is taken from [Z/H] and Z(ISM) is inferred from 12+log(O/H). Having Z(ISM) > Z(stars) is consistent with our understanding of star formation and evolution: stars cannot have abundances that are larger than those of the gas from which they formed. The plot in Figure 17 suggests that O/H abundance in the nuclear ISM is similar for all of our sample galaxies, irrespective of the luminosity averaged ages and stellar abundances inside $r_e/8$. We regard this result as significant. Denicoló, Terlevich & Terlevich (2002) showed that the relation N2 to O/H exists for either black-body or power-law photoionization. There are several sources of scatter in that relation: variations of the photoionization parameter, shape of the ionizing continuum, differences in secondary production of N, to site a few. What is important from the present result is the apparent *lack* of scatter suggesting a uniformity of the central ISM composition irrespective of the mass of the galaxy. If this result is confirmed with a larger sample of galaxies, one of the consequences of it would be to rule out galaxy mass related IMF variations.

In other words, we can interpret it as if chemical evolution has finished in these galaxies, i.e., most stars have already ejected metals to the ISM and, in general, any currently ongoing star formation in these galaxies should occur on a small scale. This is an interesting idea, and could be what distinguishes most of the chemical characteristics from early-type to late-type galaxies.

Table 4. Oxygen abundance and [Z/H] for early-type galaxies.

Galaxy	12+log(O/H)	error	[Z/H]	EW(Hα)	er(Hα)	EW([N II])	er([N II])
NGC 584	9.376	0.146	0.435	-0.244	0.081	-0.287	0.018
NGC 821	9.318	0.196	0.480	-0.316	0.093	-0.226	0.077
NGC 1407	9.242	0.075	0.690	-0.531	0.085	-0.125	0.008
NGC 1600	9.263	0.198	0.690	-0.545	0.091	-0.233	0.099
NGC 1700	9.376	0.091	0.498	-0.389	0.081	-0.518	0.013
NGC 1726	9.277	0.118	0.362	-0.800	0.166	-0.868	0.153
NGC 2300	9.498	0.295	0.530	-0.155	0.093	-0.380	0.122
NGC 2418	9.164	0.037	0.569	-1.118	0.091	-1.356	0.037
NGC 2768	9.032	0.036	0.381	-1.317	0.097	-1.594	0.065
NGC 2872	9.312	0.289	0.350	-0.256	0.115	-0.162	0.080
NGC 3156	9.321	0.095	-0.170	-0.702	0.153	-0.964	0.022
NGC 3245	8.168	0.038	0.318	-1.806	0.083	-1.643	0.121
NGC 3379	9.276	0.096	0.150	-0.435	0.085	-0.198	0.020
NGC 3599	9.400	0.078	0.422	-0.665	0.107	-1.602	0.129
NGC 3607	9.217	0.034	0.690	-1.022	0.080	-2.206	0.020
NGC 3608	9.284	0.136	0.357	-0.389	0.087	-0.190	0.042
NGC 3665	8.401	0.024	0.690	-2.122	0.083	-1.150	0.046
NGC 3941	9.289	0.063	0.585	-0.663	0.084	-0.560	0.040
NGC 4125	8.956	0.034	0.317	-1.264	0.087	-2.644	0.098
NGC 4261	9.480	0.105	0.437	-0.493	0.115	-1.438	0.102
NGC 4374	9.034	0.037	0.505	-1.308	0.107	-1.633	0.040
NGC 4550	9.196	0.135	0.290	-1.048	0.136	-0.268	0.076
NGC 5322	9.372	0.092	0.690	-0.391	0.082	-0.503	0.015
NGC 5353	9.207	0.049	0.690	-1.029	0.090	-1.417	0.102
NGC 5354	9.256	0.266	0.041	-0.464	0.086	-0.144	0.084
NGC 5444	9.301	0.132	0.192	-0.539	0.094	-0.418	0.104
NGC 5813	9.275	0.095	0.271	-0.784	0.092	-0.773	0.143
NGC 5845	9.310	0.118	0.690	-0.418	0.095	-0.305	0.045
NGC 5846	9.181	0.039	0.337	-1.075	0.086	-1.824	0.078
NGC 6172	9.377	0.058	0.250	-0.729	0.092	-1.742	0.082
NGC 7302	9.610	0.695	0.332	-0.070	0.111	-0.286	0.060
NGC 7585	9.523	0.102	0.690	-0.371	0.082	-1.186	0.091
NGC 7619	9.264	0.090	0.690	-0.635	0.084	-0.334	0.053

9 CONCLUSIONS

We have applied the stellar population model of Thomas, Maraston & Bender (2003) to estimate ages, metallicities and abundance ratios in a sample of 83 early-type galaxies mostly located in low density regions.

The stellar population properties derived for each galaxy correspond to the nuclear $r_e/8$ aperture extraction. Both ellipticals and S0s in the sample show a large spread in ages (from around 1 Gyr to 15 Gyr, but many galaxies also fall out of the model grids) and metallicities (mostly from 0.0 to 0.67 dex in [Z/H]). On average, S0 galaxies are slightly younger than the elliptical galaxies by almost 3 Gyr, and present higher [Z/H] than ellipticals by approximately 0.10 dex. The average age found for the ellipticals is 5.8 $\pm$ 0.6 Gyr and the average metallicity is +0.37 $\pm$ 0.03 dex. For S0s, the average age is 3.0 $\pm$ 0.6 Gyr and $<$[Z/H]$>$ = 0.53 $\pm$ 0.04 dex. These averages were performed excluding the three Virgo cluster galaxies in the sample, and the uncertainties shown are errors of the mean.

It seems that our elliptical galaxies are in general 3-4 Gyr younger than E galaxies in the Fornax cluster (Kuntschner 1998, 2000; see Figure 15). In the Fornax cluster the E and S0 galaxies are easily distinguished in terms of age and metallicity, whereas the Es and S0s from low-density regions appear to have more homogeneous stellar population properties; i.e. the differences in age and metallicity are not so noticeable for Es and S0s of low-density regions than for Fornax.

We find that galaxies lie in a plane defined by [Z/H]=0.99log$\sigma_0$$-$0.46log$Age-1.60$, or in linear terms Z$\propto\sigma_0\cdot Age^{-0.5}$. In this work we are adding more young galaxies to the coverage of the hyperplane defined in Trager *et al.* (2000b).

Analysing [α/Fe] ratios, we can cast some light on the star formation timescale of the galaxies. More massive (larger σ_0) and older galaxies present, on average, large [α/Fe] values, and therefore, must have undergone shorter star-formation timescales.

Comparing group against field/isolated galaxies, it is still not clear that environment plays an important role in determining their stellar population history. In particular, our isolated galaxies show ages differing by more than 8 Gyr. However, we note that the cluster elliptical galaxies of Kuntschner (2000) are more uniform in Hβ (and age) than the group, field and isolated galaxies of our sample.

Finally, we attempted to draw a broad picture of galactic chemical evolution by comparing [Z/H] metallicities derived from SSP models (i.e. stellar metallicity) against

log(O/H) abundances obtained from the N2 ratio of [N II] λ6584 to Hα emission lines (i.e. ISM metallicity). The distribution of points indicates that most galaxies have Z(ISM) > Z(stars), which is consistent with chemical evolution expectations. We interpret it as if chemical evolution has finished in early-type galaxies, i.e., most stars have already ejected metals to the ISM and, in general, any currently ongoing star formation episode in these galaxies should be on a small scale.

ACKNOWLEDGEMENTS

GD would like to thank CNPq-Brazil for the PhD fellowship, INAOE for hospitality during the visits to Mexico, Selwyn College and Cambridge Philosophical Society for financial support. The authors are grateful to the INAOE Committee for telescope time for supporting this project for five consecutive semesters and to the staff at Cananea for cheerful logistic help during the observations. We thank Amâncio Friaça, Alessandro Bressan, Itziar Aretxaga and Olac Fuentes for several interesting discussions and for clarification on the Monte Carlo technique and PCA analysis; Max Pettini and Alfonso Aragón-Salamanca for substantial comments to improve this work; and an anonymous referee for a careful reading of our manuscript and for suggestions leading to a clearer paper. RJT and ET acknowledge Mexican Research Council Project grants 40018-A-1 and E32186, respectively.

REFERENCES

Arimoto N. & Yoshii Y., 1987, A&A, 173, 23
Arimoto N. & Yoshii Y., 1989, A&A, 224, 361
Arimoto N., Matsushita K., Ishimaru Y., Ohashi T., Renzini A., 1997, ApJ, 477, 128
Bressan A., Chiosi C. & Fagotto F., 1994, ApJS, 94, 63
Bressan A., Chiosi C. & Tantalo R., 1996, A&A, 311, 425
Bruzual G. & Charlot S., 1993, ApJ, 405, 538
Burstein D., Bertola F., Buson L.M., Faber S.M., Lauer T.R., 1988, ApJ, 328, 440
Caldwell N., Rose J.A. & Concannon K.D., 2003, AJ, 125, 2891
Carollo C.M. & Danziger I.J., 1994, MNRAS, 270, 743
Cimatti A., Daddi E., Mignoli M., Pozzetti L., Renzini A., Zamorani G., Broadhurst T., Fontana A., Saracco P., Poli F., Cristiani S., D'Odorico S., Giallongo E., Gilmozzi R., Menci, N., 2002, A&A, 381, L68
Chiosi C. & Carraro G., 2002, MNRAS, 335, 335
Davies R.L., Sadler E.M., Peletier R.F., 1993, MNRAS, 262, 650
de Jong R.S. & Davies R.L., 1997, MNRAS, 285, 1L
Denicoló G., Terlevich R., Terlevich E., 2002, MNRAS, 330, 69
Denicoló G., Terlevich R., Terlevich E., Forbes, D.A., Terlevich A., Carrasco L., 2004, MNRAS, in press, (Paper I)
Einsel C., Alvensleben U.F., Krueger H., Fricke K.J., 1995, A&A, 296, 347
Ferreras I., Charlot S., Silk J., 1999, ApJ, 521, 81
Fisher D., Franx M., Illingworth G., 1995, ApJ, 448, 119
Fisher D., Franx M., Illingworth G., 1996, ApJ, 459, 110
Forbes D.A., Franx M., Illingworth G.D., 1995, ApJ, 446, 594
Forbes D.A. & Ponman T.J., 1999, MNRAS, 309, 623
Garcia A.M., 1993, A&AS, 100, 47
Gibson B., 1996, ApJ, 468, 167 (1996a)
Gibson B., 1996, MNRAS, 278, 829 (1996b)
Gibson B., 1998, ApJ, 501, 675
Gibson B. & Matteucci F., 1997, ASP Conference Series, 117, 435
González J.J., 1993, PhD thesis, Univ. California
Goudfrooij P., Hansen L., Jørgensen H.E., Norgaard-Nielsen K.U., de Jong T., van den Hoek L.B., 1994, A&AS, 104, 179
Grevesse N., Noels A. & Sauval A.J., 1996, in S.S. Holt & G. Sonneborn (eds.), *Cosmic Abundances*, Astr. Soc. Pacific Conf. Series, p. 177
Jablonka P., Martin P., Arimoto N., 1996, AJ, 112, 1415
Jørgensen I., 1999, MNRAS, 306, 607
Kauffmann G., White S.D.M. & Guiderdoni B., 1993, MNRAS, 264, 201
Kuntschner H., 1998, PhD thesis, Univ. of Durham
Kuntschner H., 2000, MNRAS, 315, 184 (K00)
Kuntschner H., Lucey J.R., Smith R.J., Hudson M.J. & Davies R.L., 2001, MNRAS, 323, 615
Loewenstein M. & Mushotzky R.F., 1996, ApJ, 471, 83
Longhetti M., Rampazzo R., Bressan A. & Chiosi C., 1998, A&AS, 130, 251 (1998a)
Longhetti M., Rampazzo R., Bressan A. & Chiosi C., 1998, A&AS, 130, 267 (1998b)
Longhetti M., Bressan A., Chiosi C. & Rampazzo R., 2000, A&A, 353, 917
Maraston C. & Thomas D., 2000, ApJ, 541, 126
Maraston C., Greggio L., Renzini A., Ortolani S., Saglia R.P., Puzia T.H., Kissler-Patig M., 2003, A&A, 400, 823
Matsushita K., Ohashi T., Makishima K., 2000, PASJ, 52, 685
Matteucci F. & Padovani P., 1993, ApJ, 419, 485
McWilliam A. & Rich R.M., 1994, ApJS, 91, 749
Michard R. & Marchal J., 1994, A&AS, 105, 481
Navarro J.F., Frenk C.S., White S.D.M, 1996, ApJ, 462, 563
Nomoto K., Hashimoto M., Tsujimoto T., Thielemann F.-K., Kishimoto N., Kubo Y., Nakasato N., 1997a, Nucl. Phys. A, 616, 79c
Nomoto K., Iwamoto K., Nakasato N., Thielemann F.-K., Brachwitz F., Tsujimoto T., Kubo Y., Kishimoto N., 1997b, Nucl. Phys. A, 621, 467c
O'Connell R.W., 1999, ARA&A, 37, 603
Peletier R., Davies R.L., Davis L.E., Illingworth G.D., Cawson M., 1990, AJ, 100, 1091
Poggianti B.M. & Barbaro G., 1997, A&A, 325, 1025
Press W.H., Teukolsky S.A., Vetterling W.T., Flannery B.P., 1992, Numerical Recipes - Second Edition. Cambridge Univ. Press, Cambridge
Puzia T.H., Saglia R.P., Kissler-Patig M., Maraston C., Greggio L., Renzini A., Ortolani S., 2002, A&A, 395, 45
Ravindranath S., Ho L.C., Peng C.Y., Filippenko A.V., Sargent W.L.W., 2001, AJ, 122, 653
Reid N., Boisson C., Sansom A.E., 1994, MNRAS, 269, 713
Ronen S., Aragón-Salamanca A., Lahav O., 1999, MNRAS, 303, 284
Scorza C., 1993, IAUS, 153, 425
Scorza C. & Bender R., 1990, "Morphological and Physical Classification of Galaxies", Proceedings of the 5^{th} International Workshop of the Osservatorio Astronomico di Capodimonte, Kluwer Academic Publishers, edited by G. Longo, M. Capaccioli, and G. Busarello. Astrophysics and Space Science Library, Vol. 178, p.389
Steinmetz M., 1996, IAU Symposium 171, 259
Tantalo R., Chiosi C., Bressan A., Fagotto F., 1996, A&A, 311, 361
Tantalo R., Chiosi C. & Bressan A., 1998, A&A, 333, 419
Terlevich A.I. & Forbes D.A., 2002, MNRAS, 330, 547 (TF02)
Thomas D. & Kauffmann G., 1999, ASP Conference Proceedings, 192, 261
Thomas D., Maraston C. & Bender R., 2003, MNRAS, 339, 897 (TMB03)
Thomas D., Maraston C. & Korn A., 2004, MNRAS, 351, L19
Trager S.C., 1997, PhD Thesis, Univ. of California, Santa Cruz

Trager S.C., Worthey G., Faber S.M., Burstein D. & González J.J., 1998, ApJS, 166, 1
Trager S.C., Faber S.M., Worthey G., González J.J., 2000a, AJ, 119, 1645
Trager S.C., Faber S.M., Worthey G., González J.J., 2000b, AJ, 120, 165 (T00b)
Tripicco M.J. & Bell R.A., 1995, AJ, 110, 3035
Tully R.B., 1987, Nearby Galaxy Catalog, Cambridge: Cambridge University Press
Whitney C.A., 1983, A&AS, 51, 443
Willis J.P., Hewett P.C., Warren S.J., Lewis G.F., 2002, MNRAS, 337, 953
Worthey G., 1992, Ph.D. Thesis, Univ. California, Santa Cruz
Worthey G., 1994, ApJS, 95, 107 (W94)
Worthey G., 1998, PASP, 110, 888
Worthey G., Faber S.M., González J.J., 1992, ApJ, 398, 69
Worthey G., Faber S.M., González J.J. & Burstein D., 1994, ApJS, 94, 687
Zirbel E.L., Baum S.A., 1998, ApJS, 114, 177